atoms

MDPI

Article

High-Temperature Optical Spectra of Diatomic Molecules: Influence of the Avoided Level Crossing

Robert Beuc * and Goran Pichler

Institute of Physics, 10000 Zagreb, Croatia; pichler@ifs.hr

* Correspondence: beuc@ifs.hr; Tel.: +385-091-787-5082

Received: 26 May 2020; Accepted: 10 June 2020; Published: 15 June 2020

Abstract: In this study, we analyzed the light absorption by diatomic molecules or colliding atoms in a spectral region dominated by an avoided crossing of adiabatic state levels or crossing of the corresponding diabatic state levels. Our attention was focused on the low-resolution spectrum at a higher gas temperature under local thermodynamic equilibrium conditions. The absorption measurements of mixed vapors of potassium (≈80%) and cesium (≈20%) were made in the temperature range of 542–715 K and the infrared spectral range 900–1250 nm. In this area, the main spectral contributions were the broad $A^1\Sigma^+_{(u)}\left(0^+_{(u)}\right) - X^1\Sigma^+_{(g)}\left(0^+_{(g)}\right)$ bands of K_2, Cs_2, and KCs molecules. There was a crossing of $A^1\Sigma^+_{(u)}\left(0^+_{(u)}\right)$ and $b^3\Pi_{(u)}\left(0^+_{(u)}\right)$ state potential curves and the coupling of this state was due to the matrix element $\left\langle A^1\Sigma^+_{(u)}\left(0^+_{(u)}\right)\middle|H_{so}\middle|b^3\Pi_{(u)}\left(0^+_{(u)}\right)\right\rangle$ of the spin–orbit interaction. Using data for relevant electronic potential curves and transition dipole moments existing in the literature, the spectra of the $A^1\Sigma^+_{(u)}\left(0^+_{(u)}\right) - X^1\Sigma^+_{(g)}\left(0^+_{(g)}\right)$ molecular bands of K_2, Cs_2, and KCs molecules were calculated. Full quantum mechanical and semi-quantum coupled channel calculations were done and compared with their non-coherent adiabatic or diabatic approximations. Through the comparison of our theoretical and experimental spectra, we identified all observed spectral features and determined the atoms' number density and gas temperature.

Keywords: diatomic molecules; optical spectra; spin-orbit coupling; non-adiabatic transitions; thermodynamic equilibrium

1. Introduction

Several approaches to the theoretical simulation of low-resolution, high-temperature optical spectra of diatomic molecules under local thermodynamic equilibrium conditions have been analyzed in detail by Beuc et al. [1]. Using relevant data for molecular potential curves and transition dipole moments, theoretical simulations can be powerful tools for identifying spectral features, gas temperatures, and atom number densities. Whereas in Beuc et al. [1], the optical transition between two well-isolated adiabatic states is analyzed, in this paper, the photon absorption from the lower adiabatic state into two excited non-radiative coupled electronic states is studied.

Many years ago, Devdariani et al. [2–4] and O'Callaghan et al. [5] studied this problem within semiclassical theory using a Landau-Zener approximation [6,7]. Although their analysis focused on the absorption and emission of light by colliding atoms, their conclusions can be qualitatively applied when interpreting quantum mechanical calculations of bound–bound molecular transitions.

The focus of this study was the spectral phenomenon that exists for all alkali metal homo- and hetero-nuclear molecular spectra. On the red side of the first resonant atomic transition doublet, the spectrum is dominated by molecular $A^1\Sigma^+_{(u)}\left(0^+_{(u)}\right) - X^1\Sigma^+_{(g)}\left(0^+_{(g)}\right)$ bands (shorter $A - X$ bands).

The brackets in the sub-script contain the gerade or ungerade symmetry mark, which is valid only for homo-nuclear molecules. The potential curve of the singlet $A^1\Sigma^+_{(u)}\left(0^+_{(u)}\right)$ state crosses with the potential curve of one component $b^3\Pi_{(u)}\left(0^+_{(u)}\right)$ of the triplet electronic state $b^3\Pi_{(u)}\left(\Omega^{(+,-)}_{(u)}\right)$. These electronic states are coupled by the matrix element $\left\langle A^1\Sigma^+_{(u)}\left(0^+_{(u)}\right)\middle|H_{so}\middle|b^3\Pi_{(u)}\left(0^+_{(u)}\right)\right\rangle$ of the spin-orbit (SO) interaction, which has as a consequence the perturbation of the $A-X$ spectrum.

For several decades, low-resolution spectra of the $A-X$ band at high temperatures have been widely experimentally and theoretically investigated, for example: Li_2 [8–11], Na_2 [1,8,11,12], K_2 [11–15], Rb_2 [16], and Cs_2 [1,5,17,18]. The influence of $A^1\Sigma^+_{(u)}\left(0^+_{(u)}\right) - b^3\Pi_{(u)}\left(0^+_{(u)}\right)$ coupling is directly observed only in the case of the heavy alkali dimers Rb_2 and Cs_2 due to their large SO interaction.

Many more studies of $A^1\Sigma^+_{(u)}\left(0^+_{(u)}\right) - b^3\Pi_{(u)}\left(0^+_{(u)}\right)$ mixing in alkali dimer spectra have been done using high-resolution spectroscopic techniques, such as laser-induced fluorescence Fourier transform spectroscopy and optical–optical double resonance polarization spectroscopy. By using deperturbation analysis, accurate spectroscopic data have reproduced the potential curves of $A^1\Sigma^+_{(u)}\left(0^+_{(u)}\right)andb^3\Pi_{(u)}\left(0^+_{(u)}\right)$ electronic states and coupling matrix element $\left\langle A^1\Sigma^+_{(u)}\left(0^+_{(u)}\right)\middle|H_{so}\middle|b^3\Pi_{(u)}\left(0^+_{(u)}\right)\right\rangle$ in the case of homonuclear dimers K_2 [19–21], Rb_2 [22,23], and Cs_2 [24,25], and heteronuclear dimers LiCs [26,27], NaCs [28], RbCs [29,30], and KCs [31–33]. In these theoretical analyses of spectroscopic data, the rotational couplings of $b^3\Pi_{(u)}\left(\Omega^{(+,-)}_{(u)}\right)$ state components whose angular moments Ω differ by 1 are included. The theoretical analysis in this study was focused on the low-resolution spectrum; therefore, this type of coupling can be neglected.

To our knowledge, there is no study of the high-temperature low-resolution $A-X$ spectra of heteronuclear dimers in the literature. We measured the absorption spectrum of a potassium and cesium vapor mixture at temperatures of 542–715 K. In the infrared spectra from 900–1250 nm, the dominant contributions were the $A-X$ bands of K_2, Cs_2, and KCs dimers. Using existing relevant potential curves and transition dipole moments obtained by quantum chemical calculations and the analysis of spectroscopic data, we calculated theoretical spectra in the measured wavelength range. We compared coupled channel quantum mechanical spectra calculations with coupled channel semi-quantum calculations and showed that a time-efficient semi-quantum approach yielded results comparable to a full quantum approach. Using semi-classical theory [2–5], we defined the conditions under which coupled channel calculations can be approximated by non-coherent adiabatic or diabatic approximations.

By comparing the experimental absorption coefficients with the theoretical simulations, we determined the temperature and potassium and cesium number densities in the gas mixture. The numerically time-efficient semi-quantum coupled channel calculus gave satisfactory good low-resolution spectra for K_2, Cs_2, and KCs dimers and can be used as an efficient alkali gas diagnostic tool.

2. Theoretical Background and Methods

The total Hamiltonian of a diatomic molecule is $H(\mathbf{r},\mathbf{R}) = T_R + H^{el}(\mathbf{r},\mathbf{R})$, wherein $T_R = -\frac{\hbar^2}{2\mu}\Delta_R$ is the nuclei kinetic energy operator and μ is the molecular reduced mass. $H^{el}(\mathbf{r},\mathbf{R})$ is the electronic part of the Hamiltonian containing the electron kinetic energy operator, all electrostatic interactions in a molecule, and the spin–orbit interaction, all of which depend on the interatomic distance R and positions vectors of all electrons **r**. The eigenvector of the Hamiltonian $H(\mathbf{r},\mathbf{R})$ is the function:

$$\Psi_M(\mathbf{r},\mathbf{R}) = \sum_i \phi_i(\mathbf{r},\mathbf{R}))\psi_{iM}(R), \quad (1)$$

which is represented as a sum of the product of the wavefunctions $\phi_i(\mathbf{r},\mathbf{R})$ that describe electrons and the functions $\psi_{iM}(\mathbf{R})$ that describe the motion of the atoms. By including the wavefunctions $\Psi_M(\mathbf{r},\mathbf{R})$ into the Schrödinger equation, one obtains a series of coupled equations:

$$\Big(T_R + H_{ii}^{el}(R) + X_{ii}(\mathbf{R}) - E\Big)\psi_{iM}(\mathbf{R}) \;=\; -\sum_{j\neq i}\Big(H_{ij}^{el}(R) + X_{ij}(\mathbf{R})\Big)\psi_{jM}(\mathbf{R}), \tag{2}$$

where $H_{ij}^{el}(R) \;=\; \Big\langle \phi_i(\mathbf{r},R)\Big|H^{el}\Big|\phi_j(\mathbf{r},R)\Big\rangle$, $X_{ij}(\mathbf{R}) \;=\; \Big\langle \phi_i(\mathbf{r},R)\Big|T_R\Big|\phi_j(\mathbf{r},R)\Big\rangle - \frac{\hbar^2}{2\mu}\Big\langle \phi_i(\mathbf{r},R)\Big|\nabla_R\Big|\phi_j(\mathbf{r},R)\Big\rangle\nabla_R$. In a spherical coordinate system, X_{ij} can be written as $X_{ij} \;=\; X_{ij}^R + X_{ij}^A$, where X_{ij}^R depends on electronic wavefunction changes related to the interatomic distance R and X_{ij}^A depends on changes related to the rotation of the molecule (for details, see Janev et al. [34]). The functions $\phi_i(\mathbf{r},\mathbf{R})$ belong to a complete set of orthogonal normalized functions that can be chosen in various ways.

The adiabatic representation is a uniquely defined base of wavefunctions that diagonalize the electronic Hamiltonian $H_{ij}^{el}(R) \;=\; V_i^a(R)\delta_{i,j}$. In the adiabatic representation, Equation (2) has the form:

$$(T_R + V_i(R) + X_{ii}(\mathbf{R}) - E)\psi_{iM}(\mathbf{R}) \;=\; -\sum_{j\neq i} X_{ij}(\mathbf{R})\psi_{jM}(\mathbf{R}). \tag{3}$$

Potential curves $V_i(R)$ for adiabatic states of the same symmetry cannot intersect (Wigner-Neuman theorem) and they avoid crossing. In the region of avoided crossing, adiabatic states of the same symmetry are coupled by the matrix element X_{ij}^R (radial coupling). Note that the adiabatic or diabatic states whose electronic angular momentum Ω differ by 1 are coupled by the matrix element X_{ij}^A (angular coupling). In the region where one can neglect all matrix elements X_{ij} (Born-Oppenheimer adiabatic approximation BOA), Equation (2) has the simple form:

$$(T_R + V_i(R) - E)\psi_{iM}(\mathbf{R}) \;=\; 0, \tag{4}$$

and the molecular wave function has the simple form $\Psi_M(\mathbf{r},\mathbf{R}) \;=\; \phi_i(\mathbf{r},R)\psi_{iM}(\mathbf{R})$. Please note, in the case of molecules with large reduced masses, which is true for the dimers analyzed in this paper, the $X_{ii}(\mathbf{R})$ matrix elements are negligible.

The diabatic representation according to Lichten [35] is the base of electronic wavefunctions for which the matrix elements X_{ij} are negligible ($X_{ij} << 1$) and the Equation (2) has the simple form $\Big(T_R + V_i^d(R) - E\Big)\psi_{iM}(\mathbf{R}) \;=\; -\sum_{j\neq i} H_{ij}^{el}(R)\psi_{iM}(\mathbf{R})$, where $V_i^d(R) \;=\; H_{ii}^{el}(R)$. The diabatic base for which $X_{ij}^R(R) \;=\; 0$ is called the radial diabatic base. Smith [36] has shown that the adiabatic and the radial diabatic base are connected through a unitary transformation. Unlike the uniquely defined adiabatic base, there is a class of radial diabatic bases that can be obtained using a unitary transformation (R independent) of one of them. In this study, we chose a diabatic base that diagonalized the electronic Hamiltonian at small interatomic distances.

The probability of an optical transition between the lower energy molecular state M'' and higher energy state M' is proportional to the square of the molecular dipole moment $\hat{\mathbf{D}}(r,R)$ matrix element:

$$\sigma_{M''}^{M'} \;\propto\; \Big|\big\langle \Psi_{M''}(\mathbf{r},\mathbf{R})\big|\hat{\mathbf{D}}(r,R)\big|\Psi_{M'}(\mathbf{r},\mathbf{R})\big\rangle\Big|^2 \;=\; \left|\sum_{i,j}\big\langle \psi_{iM''}(\mathbf{R})\big|\mathbf{D}_{ij}(R)\big|\psi_{jM'}(\mathbf{R})\big\rangle\right|^2, \tag{5}$$

where $\mathbf{D}_{ij}(R) \;=\; \Big\langle \phi_i(\mathbf{r},\mathbf{R})\Big|\hat{\mathbf{D}}(r,R)\Big|\phi_j(\mathbf{r},\mathbf{R})\Big\rangle$ is the electronic dipole moment for the transition between the adiabatic or diabatic states i and j.

2.1. One Excited Electronic State

If one assumes that the conditions for the Born-Oppenheimer approximation are satisfied, the wave function of the molecular state is given by one product of the nuclear and electronic wave function $\Psi_{vJ\Lambda}(\mathbf{r},\mathbf{R}) = \phi_\Lambda(\mathbf{r},R)\psi_{vJ\Lambda}(\mathbf{R})$. Here, the electronic state is labeled with Λ (Λ usually refers to the axial component of the electronic angular momentum). The motion of the atoms is characterized by vibrational v and rotational J quantum numbers. After the separation of the variables, the rovibrational wavefunction can be expressed as a product of the rotational and vibrational wavefunctions $\psi_{vJ\Lambda}(\mathbf{R}) = \mathfrak{R}_J(\theta,\varphi)\frac{1}{R}\varphi_{vJ\Lambda}(R)$. The Schrödinger equation for the vibrational wavefunction is:

$$\left(E_{vJ\Lambda} - V_\Lambda(R) - \frac{\hbar^2}{2\mu}\frac{J(J+1)-\Lambda^2}{R^2} + \frac{\hbar^2}{2\mu}\frac{d^2}{dR^2}\right)\varphi_{vJ\Lambda}(R) = 0, \quad (6)$$

where $V_\Lambda(R)$ is the electronic potential of the electronic state Λ. The same equation gives the energies $E_{\varepsilon J\Lambda}$ and the energy-normalized wavefunctions $\phi_{\varepsilon J\Lambda}$ of the free states.

The spectra of the averaged absorption from the lower Λ'' to the upper Λ' electronic state comprise contributions from the transitions between all rovibrational states of a lower (v'', J'', Λ'') and the upper (v', J', Λ') electronic state.

The absorption cross-section for the transition from a rovibrational state (v'', J'', Λ'') to the rovibrational state (v', J', Λ') is [8,9]:

$$\sigma^{v'J'\Lambda'}_{v''J''\Lambda''}(\nu) = \frac{8\pi^3\nu}{3hc}\frac{2-\delta_{0,\Lambda'+\Lambda''}}{2-\delta_{0,\Lambda''}}\frac{S^{J'\Lambda'}_{J''\Lambda''}}{2J''+1}\left|\left\langle\varphi_{v''J''\Lambda''}\left|\mathbf{D}(R)\right|\varphi_{v'J'\Lambda'}\right\rangle\right|^2 g(\nu-\nu_{tr}), \quad (7)$$

where $\mathbf{D}(R) = \left\langle\phi_{\Lambda''}(\mathbf{r},\mathbf{R})\left|\hat{\mathbf{D}}(r,R)\right|\phi_{\Lambda'}(\mathbf{r},\mathbf{R})\right\rangle$ is the electronic transition dipole moment, $g(\nu-\nu_{tr})$ is the line-shape function, $h\nu_{tr} = E_{v',J,\Lambda'} - E_{v'',J,\Lambda''}$ is the transition energy, and $S^{J'\Lambda'}_{J''\Lambda''}$ is the Hönl–London factor. At thermodynamic equilibrium, the reduced absorption coefficient is [8,9,12]:

$$k(\nu,T) = C(\Lambda'',T)\nu\sum_{v''v'J''J'}\frac{\omega_{J''}}{\overline{\omega}_J}\exp\left(-\frac{E_{v''J''\Lambda''}}{k_BT}\right)S^{J'\Lambda'}_{J''\Lambda''}\left|\left\langle\varphi_{v''J''\Lambda''}\left|\mathbf{D}(R)\right|\varphi_{v'J'\Lambda'}\right\rangle\right|^2 g(\nu-\nu_{ij}). \quad (8)$$

$C(\Lambda'',T)$ is a statistical factor that depends on the symmetry of the electronic states and the temperature:

$$C(\Lambda'',T) = \frac{\overline{\omega}_J}{3hc}\frac{2-\delta_{0,\Lambda'+\Lambda''}}{2-\delta_{0,\Lambda''}}\frac{(2S+1)(2\Lambda''+1)}{(2S_A+1)(2L_A+1)(2S_B+1)(2L_B+1)}\left(\frac{2\pi}{\mu kT}\right)^{3/2}, \quad (9)$$

where $S_{A,B}$ is the spin and $L_{A,B}$ is the angular momentum of atom A, B. ω_J is a statistical factor that depends on the atomic nuclear spin and parity of the molecular angular momentum J with the averaged value $\overline{\omega}_J = \frac{1}{2}$ for the homonuclear molecules and $\overline{\omega}_J = 1$ for heteronuclear molecules.

In each electronic state Λ, there is a finite number of bound and quasi-bound states with unity-normalized wavefunctions $\varphi_{vJ\Lambda}$ and an infinite continuum of free rovibrational states with energy-normalized wavefunctions $\phi_{\varepsilon J\Lambda}$. Therefore, the sum over the rovibrational transitions in Equation (8) formally includes the integration over the bound-free, free-bound, and bound-bound transitions.

To calculate the energies and wavefunctions of rovibrational states, the FGH method (Fourier grid Hamiltonian) is used, where functions are represented on a finite number of grid points R_i (i = 1, ... , N) [37]. On the grid of uniformly spaced points, where $\delta R = R_{i+1} - R_i$ for the electronic state S with an electronic angular moment L and electronic potential V_P, the $N \times N$ Hamiltonian matrix is defined as:

$$H_{J,L,S} = \frac{\hbar^2}{2\mu}\begin{Bmatrix} \frac{1}{\delta R^2}\left(\frac{\pi^2}{3}-\frac{1}{2i^2}\right)+\frac{J(J+1)-L^2}{{R_i}^2} & i=j \\ (-1)^{i-j}\frac{1}{\delta R^2}\frac{8ij}{(i^2-j^2)^2} & i\neq j \end{Bmatrix}+\begin{Bmatrix} V_S(R_i) & i=j \\ 0 & i\neq j \end{Bmatrix}. \quad (10)$$

Energies $E_{v,J,L,S}$ and radial wavefunctions $\varphi_{v,J,L,S}$ can be determined using the diagonalization of the Hamiltonian matrix $H_{J,L,S}$. Eigenvalues of the matrix $H_{J,L,S}$ represent the energies of rovibrational states and eigenvectors of the Hamiltonian matrix containing the corresponding unity-normalized wavefunction on the grid points. This method, in addition to the bound-state energies, gives a discrete set of free-state continuum energies, but in the range spanned by the grid, the corresponding unity-normalized wavefunctions do represent the states of a continuum.

The quantum calculation (QC) of spectra using Equation (8) are time-consuming and therefore not suitable for fast diagnoses (see the discussion in Beuc et al. [1]). If one needs to analyze low-resolution spectra using the Q-branch approximation (only $J'' \rightarrow J''$ transitions) by replacing the summation over J'' with the summation over the k_M intervals containing n neighbor J'' values, the efficient form of the reduced absorption coefficient is [1]:

$$k(\nu,T) = C(\Lambda'',T)\nu \sum_{v''=0,v'=0,k=0}^{N,N,k_M} n[2(kn+\Lambda)+n]\exp\left(-\frac{E_{v''J_k\Lambda''}}{k_BT}\right)\left|\left\langle\varphi_{v''J_k\Lambda''}\left|\mathbf{D}(R)\right|\varphi_{v'J_k\Lambda'}\right\rangle\right|^2\overline{g}(\nu-\nu_{tr_k}). \quad (11)$$

The number of intervals k_M is the nearest integer of N/n, Λ is the larger value of Λ'' and Λ', and $J_k(J_k+1) = (kn+\Lambda)(kn+\Lambda+n)+\frac{1}{2}(n^2-1)$. In this study, we use the absorption coefficient in Equation (11) in the wavelength domain as a QC result:

$$k(\lambda,\Delta\lambda,T) = C(\Lambda'',T)\frac{\lambda}{\Delta\lambda}\sum_{v''=0,v'=0,k=0}^{N,N,k_M} n[2(kn+\Lambda)+n]\exp\left(-\frac{E_{v''J_k\Lambda''}}{k_BT}\right)\left|\left\langle\varphi_{v''J_k\Lambda''}\left|\mathbf{D}(R)\right|\varphi_{v'J_k\Lambda'}\right\rangle\right|^2 H(\lambda,\Delta\lambda,\lambda_{tr}) \quad (12)$$

In the above equation, the line profile $g(\lambda-\lambda_{tr}^{(i)})$ is approximated with a Heaviside pi (or boxcar) function $H(\lambda,\Delta\lambda,\lambda_{tr}) = \begin{cases} 1 & \lambda_{tr}\in(\lambda-\Delta\lambda,\lambda+\Delta\lambda) \\ 0 & \lambda_{tr}\notin(\lambda-\Delta\lambda,\lambda+\Delta\lambda) \end{cases}$, where the optical transition wavelength is $\lambda_{tr} = c/\nu_{tr}$ and $\Delta\lambda$ is equal to or larger than the line profile half-width and smaller than the instrumental profile half-width.

Semi-quantum approximation (SQA) [1,15] give an even faster algorithm for calculating the low-resolution reduced absorption coefficient, which in the wavelength domain, has a form:

$$k(\lambda,\Delta\lambda,T) = C(\Lambda'',T)\frac{\lambda}{\Delta\lambda}\frac{2\mu k_BT}{\hbar^2}\sum_{v'',v'}^{N,N}\exp\left(-\frac{E_{v''\bar{J}\Lambda''}}{k_BT}\right)\left|\left\langle\varphi_{v'',\bar{J},\Lambda''}\left|R\mathbf{D}(R)\right|\varphi_{v',\bar{J},\Lambda'}\right\rangle\right|^2 H(\lambda,\Delta\lambda,\lambda_{tr}), \quad (13)$$

where $\bar{J}$ is equal to the larger value of Λ'' and Λ'. This expression was formally obtained using a completely semi-classical procedure but was in a quantum-like form. An evaluation of the applicability, accuracy, and numerical efficiency of Equations (8), (11), (12), and (13) was extensively discussed in Beuc et al. [1].

One can describe the radial movement of atoms using a classical trajectory $R = R(t)$ with the radial velocity $v_r(t) = \sqrt{\frac{2}{\mu}\left(E-V_\Lambda(R(t))-E\frac{\rho^2}{R(t)^2}\right)}$, where E is the energy of the molecule and ρ is the collision impact parameter. The wavefunction of the molecule in the electronic state Λ'' "dressed" [38] with photon frequency ν is $\Psi_{E\rho\Lambda''}(r,t) = \Phi_{\Lambda''}(r,R(t))\exp\left(-\frac{i}{\hbar}\int_{-\infty}^{t}dt'[V''(R(t'))+h\nu]\right)$ and the wavefunction of the molecule in

the excited state Λ' is $\Psi_{E\rho\Lambda'}(r,t) = \Phi_{\Lambda'}(r,R(t))\exp\left(-\frac{i}{\hbar}\int_{-\infty}^{t} dt' V'(R(t'))\right)$. The absorption cross-section of the optical transition between the lower ($E\rho\Lambda''$) and the upper ($E\rho\Lambda'$) molecular state is:

$$\sigma_{E\rho\Lambda''}^{E\rho\Lambda'} \propto \left|\int_{-\infty}^{\infty} dt \langle \Phi_{\Lambda''}(r,R)\left|\hat{\mathbf{D}}(r,R)\right|\Phi_{\Lambda'}(r,R)\rangle \exp\left(-\frac{i}{\hbar}\int_{-\infty}^{t} dt'\left[V''(R(t')) + h\nu - V'(R(t'))\right]\right)\right|^2. \quad (14)$$

At thermodynamic equilibrium, the reduced absorption coefficient is given by the averaged absorption cross-section over parameters of the statistical ensemble E and ρ:

$$k(\nu, T) = C(\Lambda'', T)\frac{64\pi^2}{h^3}\nu \int_{\varepsilon''_{\min}}^{\infty} dE \cdot E \exp(-\frac{E}{k_B T}) \int_0^{\infty} d\rho \cdot \rho \left|\int_{-\infty}^{\infty} dt \mathbf{D}(t) \exp\left[\frac{1}{\hbar}\int_0^t (\Delta(t\prime) - h\nu)\, dt'\right]\right|^2, \quad (15)$$

where $\Delta(R(t)) = V_{\Lambda'}(R(t)) - V_{\Lambda''}(R(t))$ is the electronic transition difference potential.

The non-coherent quasi-static approximation is done using the first-order stationary phase approximation of the time-dependent integral in Equation (15), partial integration over ρ, and neglecting the rapidly oscillating terms [1,39]:

$$k(\nu, T) = B(\Lambda'')\nu \sum_{i=1}^{n} \frac{R_i^2 D(R_i)^2}{\left|\Delta'(R_i)\right|} \exp(-\frac{V_{\Lambda''}(R_i)}{k_B T}), \quad (16)$$

where $\Delta'(R) = \frac{d}{dR}\Delta(R)$, $B(\Lambda'') = \frac{\pi\sqrt{2}}{3\hbar^3 c}\overline{\omega}_J \frac{2-\delta_{0,\Lambda'+\Lambda''}}{2-\delta_{0,\Lambda''}} \frac{(2S+1)(2\Lambda''+1)}{(2S_A+1)(2L_A+1)(2S_B+1)(2L_B+1)}$, and the summation is over all real Condon points R_i satisfying $\Delta(R_i) = h\nu$. This approximation gives a good description of the spectra but diverges at the difference potential extremes, which are most often the consequence of the avoided crossing of the adiabatic electronic states' potential curves.

In the case where the difference potential has only one extreme point R_e, a coherent uniform Airy approximation of the spectral profile is defined [1,39]. In the classically allowed region, the reduced absorption coefficient has the form:

$$k(\nu, T) = B(\Lambda'')\nu \left\{ \begin{array}{l} \left[\frac{R_1^2 D(R_1)^2}{|\Delta'(R_1)|}\exp(-\frac{V_{\Lambda''}(R_1)}{k_B T}) + \frac{R_2^2 D(R_2)^2}{|\Delta'(R_2)|}\exp(-\frac{V_{\Lambda''}(R_2)}{k_B T})\right] 3\sqrt{\pi}(\sqrt{z}L(z) + \frac{1}{\sqrt{z}}H(z)) \\ +2\frac{R_1{}^2 D(R_1) D(R_2)}{\sqrt{|\Delta'(R_1)||\Delta'(R_2)|}}\exp(-\frac{V_{\Lambda''}(R_1)}{k_B T}) 3\sqrt{\pi}(\sqrt{z}L(z) - \frac{1}{\sqrt{z}}H(z)) \end{array} \right\}, \quad (17)$$

where R_1 and R_2 are the Condon points satisfying $\Delta(R_{1,2}) = h\nu$, and the mapping parameter is $z = z(\nu, T) = \left(\frac{\mu}{2k_B T}\right)^{\frac{1}{3}}\left(\frac{3\mathrm{sgn}[\Delta''(R_e)]}{4\hbar}\int_{R_1}^{R_2} dR(\Delta(R) - h\nu)\right)^{\frac{2}{3}}$. The functions $L(z) = \int_0^{\infty} dx \frac{Ai[-zx]^2}{x^2}\exp\left(-1/x^3\right)$ and $H(z) = \int_0^{\infty} dx \frac{Ai\prime[-zx]^2}{x^3}\exp\left(-1/x^3\right)$ are integrals of the square of the Airy function and its first derivative, respectively. The uniform Airy approximation can be extended to the case where the transition difference potential has several extremes [1].

2.2. Two Coupled Excited Electronic States

In this paragraph, an optical transition from the ground electronic state Λ'' satisfying BOA to two coupled electronic states Λ'_1 and Λ'_2 is analyzed. It is assumed that the electronic wavefunction of the excited states belonging to the radial diabatic base diagonalizes the electronic Hamiltonian at small interatomic distances. The electronic wavefunction and potential for the ground state are $\Phi_{\Lambda''}(r,R)$ and $V_{\Lambda''}(R)$ for the excited states $\Phi^d_{\Lambda'_{1,2}}(r,R)$ and $V^d_{\Lambda'_{1,2}}(R)$, respectively. The excited

electronic diabatic states are coupled via the matrix element $V(R) = \left\langle \Phi^d_{\Lambda'_1}(\mathbf{r},R)\middle|H^{el}(\mathbf{r},R)\middle|\Phi^d_{\Lambda'_2}(\mathbf{r},R)\right\rangle$ and all other coupling matrix elements $X_{ij}(R)$ and $H^{el}_{ij\neq i}(R)$ are neglected. The difference potentials for the transitions between the ground and excited states are $\Delta^d_{\Lambda'_{1,2}}(R) = V^d_{\Lambda'_{1,2}}(R) - V_{\Lambda''}(R)$ and the corresponding transition dipole moments are $\mathbf{d}^d_{\Lambda'1,\Lambda'2}(R) = \langle \Phi_{\Lambda''}|\mathbf{D}(R)\middle|\Phi_{\Lambda'1,\Lambda'2}\right\rangle$. The potential curves $V^d_{\Lambda'1,\Lambda'2}(R)$ and difference potential curves $\Delta^d_{\Lambda'_{1,2}}(R)$ intersect at an interatomic distance R_c, $V^d_{\Lambda'_1}(R_c) = V^d_{\Lambda'_2}(R_c)$, and $\Delta^d_{\Lambda'_1}(R_c) = \Delta^d_{\Lambda'_2}(R_c)$.

The corresponding adiabatic states' wavefunctions $\Phi^a_{\Lambda'_{1,2}}(r,R)$ and potentials $V^a_{\Lambda'_{1,2}}(R)$ are given by diagonalizing the matrix $\begin{pmatrix} V^d_{\Lambda'_1}(R) & V(R) \\ V(R) & V^d_{\Lambda'_2}(R) \end{pmatrix}$:

$$\begin{aligned} V^a_{\Lambda'_{1,2}}(R) &= \tfrac{1}{2}\left[V^d_{\Lambda'_1}(R) + V^d_{\Lambda'_2}(R) \pm \sqrt{\Delta_d(R)^2 + 4V(R)^2}\right] \\ \Phi^a_{\Lambda'1,\Lambda'2}(r,R) &= \tfrac{1}{\sqrt{2}}\sqrt{1 \pm \tfrac{\Delta_d(R)}{\sqrt{\Delta_d(R)^2+4V(R)^2}}}\Phi^d_{\Lambda'1}(r,R) \pm \tfrac{1}{\sqrt{2}}\sqrt{1 \mp \tfrac{\Delta_d(R)}{\sqrt{\Delta_d(R)^2+4V(R)^2}}}\Phi^d_{\Lambda'2}(r,R) \end{aligned} \quad (18)$$

where $\Delta_d(R) = V^d_{\Lambda'1}(R) - V^d_{\Lambda'2}(R)$. There is a simple relationship between the diabatic state potential difference $\Delta_d(R)$ and the adiabatic state potential difference $\Delta_a(R) = \sqrt{\Delta_d(R)^2 + 4V(R)^2}$.

Difference potentials and the corresponding transition dipole moments for the transition between the ground state and excited adiabatic states are:

$$\begin{aligned} \Delta^a_{\Lambda'_{1,2}}(R) &= \tfrac{1}{2}\left[\Delta^d_{\Lambda'1}(R) + \Delta^d_{\Lambda'2}(R) \pm \sqrt{\Delta_d(R)^2 + 4V(R)^2}\right] \\ \mathbf{d}^a_{\Lambda'_{1,2}}(R) &= \tfrac{1}{\sqrt{2}}\sqrt{1 \pm \tfrac{\Delta_d(R)}{\sqrt{\Delta_d(R)^2+4V(R)^2}}}\mathbf{d}^d_{\Lambda'_1}(R) \pm \tfrac{1}{\sqrt{2}}\sqrt{1 \mp \tfrac{\Delta_d(R)}{\sqrt{\Delta_d(R)^2+4V(R)^2}}}\mathbf{d}^d_{\Lambda'_2}(R) \end{aligned} \quad (19)$$

In the neighborhood of the diabatic state potential curves' crossing point, the potential curves $V^a_{\Lambda'_{1,2}}(R)$ and difference potential curves $\Delta^a_{\Lambda'_{1,2}}(R)$ have an avoided crossing, and the transition dipole moments significantly depend on the interatomic distance. The electronic adiabatic states Λ'_1 and Λ'_2 are coupled via a radial matrix element, and their couplings with all other electronic states were assumed to be negligible.

The molecular wavefunction of the excited state $\Psi_{v'J'\Lambda'}(\mathbf{r},R)$ can be written as a sum of coupled states functions in a diabatic (d) or adiabatic (a) representation:

$$\Psi_{v'J'\Lambda'}(\mathbf{r},R) = \phi^{a,d}_{v'J'\Lambda'_1}(\mathbf{R})\Phi^{a,d}_{\Lambda'_1}(\mathbf{r},R) + \phi^{a,d}_{v'J'\Lambda'_2}(\mathbf{R})\Phi^{a,d}_{\Lambda'_2}(\mathbf{r},R). \quad (20)$$

The energies $E^{a,d}_{vJ\Lambda'}$ and rovibrational radial wavefunctions $\varphi^{a,d}_{vJ\Lambda'_{1,2}}(R)$ in both representations are the solutions of the coupled channel Schrödinger equation:

$$\begin{aligned} \left(E^{a,d}_{v'J'\Lambda'} - V^{a,d}_{\Lambda'_1}(R) - \tfrac{\hbar^2}{2\mu}\tfrac{J'(J'+1)-\Lambda'^2}{R^2} + \tfrac{\hbar^2}{2\mu}\tfrac{d^2}{dR^2}\right)\varphi^{a,d}_{v'J'\Lambda'_1}(R) &= \mathbb{C}(R)^{a,d}\varphi^{a,d}_{v'J'\Lambda'_2}(R) \\ \left(E^{a,d}_{v'J'\Lambda'} - V^{a,d}_{\Lambda'_2}(R) - \tfrac{\hbar^2}{2\mu}\tfrac{J'(J'+1)-\Lambda'^2}{R^2} + \tfrac{\hbar^2}{2\mu}\tfrac{d^2}{dR^2}\right)\varphi^{a,d}_{v'J'\Lambda'_2}(R) &= \mathbb{C}(R)^{a,d}\varphi^{a,d}_{v'J'\Lambda'_1}(R) \end{aligned} \quad (21)$$

It is assumed here that both electronic states $\Lambda'_{1,2}$ have the same electronic angular moment Λ'. The coupling matrix element in the diabatic representation is $\mathbb{C}(R)^d = V(R)$, and in the adiabatic representation, it is $\mathbb{C}(R)^a = \frac{1}{2\mu}\left\langle \phi^a_{\Lambda'_1}(\mathbf{r},R)\middle|\frac{d^2}{dR^2}\middle|\phi^a_{\Lambda'_2}(\mathbf{r},R)\right\rangle + \frac{1}{\mu}\left\langle \phi^a_{\Lambda'_1}(\mathbf{r},R)\middle|\frac{d}{dR}\middle|\phi^a_{\Lambda'_2}(\mathbf{r},R)\right\rangle\frac{d}{dR}$. To solve the coupled channel Equation (21) numerically, it is suitable to use the diabatic representation and the

FGH method [40]. Energies and radial wavefunctions can be determined via diagonalization of the $2N \times 2N$ Hamiltonian matrix:

$$H_{CC} = \begin{pmatrix} H_{J,\Lambda',\Lambda'_1} & V \\ V & H_{J,\Lambda',\Lambda'_2} \end{pmatrix}, \tag{22}$$

where $H_{J,\Lambda',\Lambda'_1}$ is an $N \times N$ matrix defined by Equation (10) and $V = \begin{Bmatrix} V(R_i) & i = j \\ 0 & i \neq j \end{Bmatrix}$ is an $N \times N$ matrix.

The absorption cross-section for the transition from a rovibrational state (v'', J'', Λ'') of the ground electronic state to the rovibrational states (v', J', Λ') of the coupled excited electronic states is:

$$\begin{aligned} \sigma^{v'J'\Lambda'}_{v''J''\Lambda''}(\nu) &\propto S^{J'\Lambda'}_{J''\Lambda''} \left| \left\langle \varphi_{v''J''\Lambda''}(R) \middle| \mathbf{d}^{a,d}_{\Lambda'_1}(R) \middle| \varphi^{a,d}_{v'J'\Lambda'_1}(R) \right\rangle + \left\langle \varphi_{v''J''\Lambda''}(R) \middle| \mathbf{d}^{a,d}_{\Lambda'_2}(R) \middle| \varphi^{a,d}_{v'J'\Lambda'_2}(R) \right\rangle \right|^2 g(\nu - \nu_{tr}) \\ &= S^{J'\Lambda'}_{J''\Lambda''} g(\nu - \nu_{tr}) \cdot \\ &\cdot \left[\left| \left\langle \varphi_{v''J''\Lambda''} \middle| \mathbf{d}^{a,d}_{\Lambda'_1} \middle| \varphi^{a,d}_{v'J'\Lambda'_1} \right\rangle \right|^2 + \left| \left\langle \varphi_{v''J''\Lambda''} \middle| \mathbf{d}^{a,d}_{\Lambda'_2} \middle| \varphi^{a,d}_{v'J'\Lambda'_2} \right\rangle \right|^2 + 2\mathrm{Re}\left(\left\langle \varphi_{v''J''\Lambda''} \middle| \mathbf{d}^{a,d}_{\Lambda'_1} \middle| \varphi^{a,d}_{v'J'\Lambda'_1} \right\rangle \left\langle \varphi_{v''J''\Lambda''} \middle| \mathbf{d}^{a,d}_{\Lambda'_2} \middle| \varphi^{a,d}_{v'J'\Lambda'_2} \right\rangle \right) \right] \end{aligned} \tag{23}$$

where the transition energy is $h\nu_{tr} = E^{a,d}_{v'J'\Lambda'} - E_{v'',J,\Lambda''}$. The reduced absorption coefficient for the transition from the lower electronic state Λ'' to the excited coupled electronic states in the adiabatic or diabatic representation can be written as:

$$k(\nu, T) = k^{a,d}_{\Lambda'_1}(\nu, T) + k^{a,d}_{\Lambda'_2}(\nu, T) + 2k^{a,d}_{\mathrm{int}}(\nu, T). \tag{24}$$

This is a full quantum mechanical coupled channel approach (QCC) in the adiabatic or diabatic representation. The first contribution represents an optical transition to the electronic state Λ'_1, the second contribution represents the transition to the electronic state Λ'_2, and third contribution represents their interference. The calculations of $k^{a,d}_{\Lambda'1}(\nu, T)$, $k^{a,d}_{\Lambda'2}(\nu, T)$, and $k^{a,d}_{\mathrm{int}}(\nu, T)$ can be done using Equations (8) or (12) by replacing $\left| \left\langle \varphi_{v''J''\Lambda''} | \mathbf{D} | \varphi_{v'J'\Lambda'} \right\rangle \right|^2$ with $\left| \left\langle \varphi_{v''J''\Lambda''} \middle| \mathbf{d}^{a,d}_{\Lambda'_1} \middle| \varphi^{a,d}_{v'J'\Lambda'_1} \right\rangle \right|^2$, $\left| \left\langle \varphi_{v''J''\Lambda''} \middle| \mathbf{d}^{a,d}_{\Lambda'2} \middle| \varphi^{a,d}_{v'J'\Lambda'2} \right\rangle \right|^2$, and $\mathrm{Re}\left(\left\langle \varphi_{v''J''\Lambda''} \middle| \mathbf{d}^{a,d}_{\Lambda'_1} \middle| \varphi^{a,d}_{v'J'\Lambda'_1} \right\rangle \left\langle \varphi_{v''J''\Lambda''} \middle| \mathbf{d}^{a,d}_{\Lambda'_2} \middle| \varphi^{a,d}_{v'J'\Lambda'_2} \right\rangle \right)$, respectively.

The same Equation (24) holds for the semi-quantum coupled channel approximation (SQCC), where in Equation (13), the transition energy is $h\nu_{tr} = E^{a,d}_{v'\bar{J}\Lambda'} - E_{v'',\bar{J},\Lambda''}$ and $\left| \langle \varphi_{v''\Lambda\Lambda''} | R\mathbf{D} | \varphi_{v'\Lambda\Lambda'} \rangle \right|^2$ is replaced by $\left| \left\langle \varphi_{vJ''\Lambda''} \middle| R\mathbf{d}^{a,d}_{\Lambda'_1} \middle| \varphi^{a,d}_{vJ\Lambda'_1} \right\rangle \right|^2$, $\left| \left\langle \varphi_{vJ''\Lambda''} \middle| R\mathbf{d}^{a,d}_{\Lambda'_2} \middle| \varphi^{a,d}_{vJ\Lambda'_2} \right\rangle \right|^2$, and $\mathrm{Re}\left(\left\langle \varphi_{vJ''\Lambda''} \middle| R\mathbf{d}^{a,d}_{\Lambda'_1} \middle| \varphi^{a,d}_{vJ\Lambda'_1} \right\rangle \left\langle \varphi_{vJ''\Lambda''} \middle| R\mathbf{d}^{a,d}_{\Lambda'_2} \middle| \varphi^{a,d}_{vJ\Lambda'_2} \right\rangle \right)$ for each contribution, respectively.

If one neglects the coupling element $\mathbb{C}(R)$, the coupled Equation (21) is simplified into two ordinary Schrödinger equations:

$$\begin{aligned} \left(\widetilde{E}^{a,d}_{v'J'\Lambda'_1} - V^{a,d}_{\Lambda'_1}(R) - \frac{\hbar^2}{2\mu} \frac{J'(J'+1) - \Lambda'^2}{R^2} + \frac{\hbar^2}{2\mu} \frac{d^2}{dR^2} \right) \widetilde{\varphi}^{a,d}_{v'J'\Lambda'_1}(R) &= 0 \\ \left(\widetilde{E}^{a,d}_{v'J'\Lambda'_2} - V^{a,d}_{\Lambda'_2}(R) - \frac{\hbar^2}{2\mu} \frac{J'(J'+1) - \Lambda'^2}{R^2} + \frac{\hbar^2}{2\mu} \frac{d^2}{dR^2} \right) \widetilde{\varphi}^{a,d}_{v'J'\Lambda'_2}(R) &= 0 \end{aligned} \tag{25}$$

Because $\widetilde{E}^{a,d}_{v'J'\Lambda'_1} \neq \widetilde{E}^{a,d}_{v'J'\Lambda'_2}$, the interference contribution similar to the one in Equation (23) is negligible and the absorption coefficient can be written as the non-coherent sum of transitions to the excited states Λ'_1 and Λ'_2:

$$k(\nu, T) = k^{a,d}_{\Lambda'_1}(\nu, T) + k^{a,d}_{\Lambda'_2}(\nu, T), \tag{26}$$

where each contribution in Equation (26) can be calculated using Equations (8) or (12) by substituting $h\nu_{tr} = \widetilde{E}^{a,d}_{v'J'\Lambda'_{1,2}} - E_{v'',J,\Lambda''}$ and replacing $\left| \left\langle \varphi_{v''J''\Lambda''} | \mathbf{D} | \varphi_{v'J'\Lambda'} \right\rangle \right|^2$ with $\left| \left\langle \varphi_{v''J''\Lambda''} \middle| \mathbf{d}^{a,d}_{\Lambda'_{1,2}} \middle| \widetilde{\varphi}^{a,d}_{v'J'\Lambda'_{1.2}} \right\rangle \right|^2$. If the adiabatic (diabatic) representation is used in Equation (26), one gets a non-coherent quantum-mechanical adiabatic (diabatic) approximation QAA (QDA) of QCC.

Equation (26) also describes an approximation of SQCC, where each contribution is calculated using Equation (13) by substituting $h\nu_{tr} = E^{a,d}_{v'\bar{J}\Lambda'_{1,2}} - E_{v'',\bar{J},\Lambda''}$ and replacing $\left|\left\langle\varphi_{v''\bar{J}\Lambda''}|\mathbf{D}|\,\varphi_{v'\bar{J}\Lambda'}\right\rangle\right|^2$ with $\left|\left\langle\varphi_{v''\bar{J}\Lambda''}\left|R\mathbf{d}^{a,d}_{\Lambda'_{1,2}}\right|\varphi^{a,d}_{v'\bar{J}\Lambda'_{1,2}}\right\rangle\right|^2$. Depending on the choice of the electronic wavefunctions' basis, one obtains a non-coherent semi quantum adiabatic SQAA or diabatic SQDA approximation

2.3. The Landau–Zener Model

To analyze the essential properties of the absorption spectrum for transitions in the neighborhood of the crossing of diabatic states' potential curves, simplifications inherent to the Landau–Zener model have been made. In the neighborhood of the crossing point R_c, the potentials of the excited diabatic states can be approximated: $V^d_{\Lambda'1,2}(R) \approx V^d_{\Lambda'1}(R_c) + \beta_{1,2}\Delta R$ (note that $V^d_{\Lambda'_1}(R_c) = V^d_{\Lambda'_2}(R_c)$), and for the potential of the ground electronic state, $V_{\Lambda''}(R) \approx V_{\Lambda''}(R_c) + \beta_0\Delta R$, where $\Delta R = R - R_c$,$\beta_{1,2} = \frac{d}{dR}V^d_{\Lambda'_{1,2}}(R)_{R=R_c}$, and $\beta_0 = \frac{d}{dR}V_{\Lambda''}(R)_{R=R_0}$. The transition difference potentials are $\Delta^d_{\Lambda'_{1,2}}(R) \approx \Delta_0 + \alpha_{1,2}\Delta R$ where $\alpha_i = \beta_i - \beta_0$ and $\Delta_0 = V^d_{\Lambda'_{1,2}}(R_c) - V_0(R_c)$. Additionally, the following approximations can be used: for the coupling matrix element, $V(R) \approx V(R_c) = V$, and for the transition dipole moments,$\mathbf{d}^d_{\Lambda'_{1,2}}(R) \approx \mathbf{d}^d_{\Lambda'_{1,2}}(R_c) = \mathbf{d}_{1,2}$.

Using the same approximation, the difference potentials for the transition between the ground and the excited adiabatic states and the corresponding transition dipole moments are:

$$\begin{gathered}\Delta^a_{\Lambda'_{1,2}}(R) \approx \Delta_0 + \tfrac{\alpha_1+\alpha_2}{2}\Delta R + s\tfrac{\alpha_1-\alpha_2}{2}\sqrt{\Delta R^2 + \tfrac{4V^2}{(\alpha_1-\alpha_2)^2}}\\ \mathbf{d}^a_{1,2}(R) \approx s\tfrac{1}{\sqrt{2}}\sqrt{1 + s\tfrac{\Delta R}{\sqrt{\Delta R^2+\frac{4V^2}{(\alpha_1-\alpha_2)^2}}}}\mathbf{d}_1 + \tfrac{1}{\sqrt{2}}\sqrt{1 - s\tfrac{\Delta R}{\sqrt{\Delta R^2+\frac{4V^2}{(\alpha_1-\alpha_2)^2}}}}\mathbf{d}_2\end{gathered} \tag{27}$$

The difference potentials curves $\Delta^a_{\Lambda'_1}(R)$ and $\Delta^a_{\Lambda'_2}(R)$ are two branches of a hyperbola. If $\alpha_1\alpha_2 > 0$, the potential curves are monotonic with only one Condon point at each frequency. When $\alpha_1\alpha_2 < 0$, the difference potential curves $\Delta_{\Lambda'_1}(x)$ and $\Delta_{\Lambda'_2}(x)$ have a minimum and a maximum, respectively, and both adiabatic states have two Condon points at each frequency.

To calculate the spectral profile in the neighborhood of the diabatic potential curves' crossing point, a satisfactory approximation is $\Delta R \approx v_r(R_c)\Delta t$, where $v_r(R_c)$ is the radial velocity at the crossing point. Using Equation (16), a non-coherent sum of the absorption coefficients for transitions to excited diabatic states is:

$$k^d(\nu, T) = B(\Lambda'')\nu R_c^2 e^{-\frac{V_0(R_c)}{k_B T}}\left(\frac{\mathbf{d}_1^2}{|\alpha_1|} + \frac{\mathbf{d}_2^2}{|\alpha_2|}\right). \tag{28}$$

This is the non-coherent semi-classical diabatic approximation (SCDA) of the spectra, which is valid in both cases $\alpha_1\alpha_2 > 0$ and $\alpha_1\alpha_2 < 0$.

In the case $\alpha_1\alpha_2 > 0$, a non-coherent sum of the semi-classical absorption coefficient for the transition to the excited adiabatic states' semi-classical adiabatic approximation (SCAA) has the form $k^a(\nu, T) = k^d(\nu, T)$.

SCAA in the case $\alpha_1\alpha_2 < 0$ can be obtained using the uniform Airy approximation (Equation (16)) [41]:

$$k^a(\nu, T) = B(\Lambda'')\nu R_c^2 e^{-\frac{V_0(R_c)}{k_B T}}\left[\left(\frac{\mathbf{d}_1^2}{|\alpha_1|} + \frac{\mathbf{d}_2^2}{|\alpha_2|}\right)L^a_d(\Omega) + 2\mathbf{d}_1\mathbf{d}_2 L^a_{\text{int}}(s\Omega)\right]. \tag{29}$$

The absorption coefficient is a function of the dimensionless reduced frequency (energy) $\Omega = \frac{\alpha_1-\alpha_2}{V\sqrt{|\alpha_1\alpha_2|}}(h\nu - \Delta_0)$ suggested in Девдарианиand Себякин [2]. The crossing of diabatic states difference potentials is at $\Omega = 0$ and the maximum and minimum of the adiabatic state difference potentials are at $\Omega = \pm 2$. The profile $L^a_d(\Omega) = I_d(\Omega) + I_d(-\Omega)$ is a symmetric

function of Ω, where $I_d(\Omega) = 3\sqrt{\pi}\left(\sqrt{\frac{(\Omega+2)z(\Omega)}{\Omega-2}}L(z(\Omega)) + \sqrt{\frac{\Omega-2}{(\Omega+2)z(\Omega)}}H(z(\Omega))\right)$, parameter $z = z(T,\Omega) = \left(\frac{3}{4}\xi\int_2^{\Omega}\sqrt{x^2-4}dx\right)^{2/3}$, and $\xi = \xi(T) = \frac{V^2}{\hbar(\alpha_1-\alpha_2)}\sqrt{\frac{\mu}{2k_BT}}$ is the Massey parameter of nonadiabatic mixing. The interference profile $L^a_{\text{int}}(\Omega) = I_i(\Omega) - I_i(-\Omega)$ is an anti-symmetric function of Ω, with $L^a_{\text{int}}(0) = 0$ and $I_i(\Omega) = 3\sqrt{\pi}\left(\sqrt{\frac{(\Omega+2)z(\Omega)}{\Omega-2}}L(z(\Omega)) - \sqrt{\frac{\Omega-2}{(\Omega+2)z(\Omega)}}H(z(\Omega))\right)$ as a consequence. The following are asymptotically valid: $L^a_d(\Omega\to\pm\infty) = 1$ and $L^a_{\text{int}}(\Omega\to\pm\infty) = 0$. In the neighborhood of the potential minimum $\Omega = 2$, parameter z has a simple form $z \approx \widetilde{z}(\Omega) = \xi^{2/3}(\Omega-2)$ such that in the classically forbidden region $\Omega \le 2$, functions $I_d(\Omega)$ and $I_i(\Omega)$ can be approximated using $I_d(\Omega) \approx 3\sqrt{\pi}\left(2\xi^{1/3}L(\widetilde{z}(\Omega)) + \frac{1}{2\xi^{1/3}}H(\widetilde{z}(\Omega))\right)$ and $I_{\text{int}}(\Omega) \approx 3\sqrt{\pi}\left(2\xi^{1/3}L(\widetilde{z}(\Omega)) - \frac{1}{2\xi^{1/3}}H(\widetilde{z}(\Omega))\right)$ by analytical continuation.

The semi-classical time-dependent molecular wavefunction in the case of two non-radiative coupled diabatic electronic states is:

$$\Psi_{E\rho\Lambda'}(\mathbf{r},t) = \Phi_{\Lambda'_1}(\mathbf{r},R(t))A_1(t)\exp\left(-\frac{i}{\hbar}\int_{-\infty}^{t}dt'V^d_{\Lambda'_1}(R(t'))\right) + \Phi_{\Lambda'_2}(\mathbf{r},R(t))A_2(t)\exp\left(-\frac{i}{\hbar}\int_{-\infty}^{t}dt'V^d_{\Lambda'_2}(R(t'))\right) \quad (30)$$

Devdariani and coworkers [2–4] and O'Callaghan et al. [5] have studied the influence of non-adiabatic electronic states mixing on the shape of the spectrum within semi-classical atomic collision theory. The atomic collision can be divided into two half-collisions: the first refers to the motion from $R \approx \infty$ to the turning point R_0, and the second from the turning point to $R \approx \infty$. Within the framework of the Landau–Zener model, each half-collision takes place over a time interval $t \in (-\infty,\infty)$, where $t = 0$ is at the crossing point R_c. The coefficients $A_{1,2}(t)$ are the solutions of the coupled equations:

$$\begin{aligned} i\hbar\tfrac{d}{dt}A_1(t) &= A_2(t)V\exp\left(\tfrac{i}{2\hbar}(\alpha_1-\alpha_2)v_ct^2\right) \\ i\hbar\tfrac{d}{dt}A_2(t) &= A_1(t)V\exp\left(\tfrac{i}{2\hbar}(\alpha_2-\alpha_1)v_ct^2\right) \end{aligned} \quad (31)$$

There are two scenarios involving a collision process: the initial conditions of the first half-collision are $|A_1(-\infty)| = 1, |A_2(-\infty)| = 0$ or $|A_1(-\infty)| = 0, |A_2(-\infty)| = 1$.

The cross-section for the transition between the lower molecular state Λ'' dressed with photon $h\nu$ to the higher state Λ' for each half-collision is:

$$\begin{aligned} \sigma^{E\rho\Lambda'}_{E\rho\Lambda''}(\nu) &\propto \left|\int_{-\infty}^{\infty}dt\left\langle\Psi_{E\rho\Lambda''}(r,t)\middle|\widehat{\mathbf{D}}(r,R(t))\middle|\Psi_{E\rho\Lambda'}(\mathbf{r},t)\right\rangle\right|^2 \\ &= \mathbf{d}_1^2\left|\int_{-\infty}^{\infty}dtA_1(t)\exp\left(i\left(\tfrac{v_c}{2\hbar}\alpha_1t^2-2\pi\nu t\right)\right)\right|^2 + \mathbf{d}_2^2\left|\int_{-\infty}^{\infty}dtA_2(t)\exp\left(i\left(\tfrac{v_c}{2\hbar}\alpha_2t^2-2\pi\nu t\right)\right)\right|^2 \\ &+2\mathbf{d}_1\mathbf{d}_2\mathrm{Re}\left(\int_{-\infty}^{\infty}dtA_1(t)\exp\left(i\left(\tfrac{v_c}{2\hbar}\alpha_1t^2-2\pi\nu t\right)\right)\int_{-\infty}^{\infty}dtA_2^*(t)\exp\left(-i\left(\tfrac{v_c}{2\hbar}\alpha_2t^2-2\pi\nu t\right)\right)\right) \end{aligned} \quad (32)$$

Both groups of authors have calculated the spectral contribution for each half-collision and both scenarios of the initial conditions. After non-coherent summation of all contributions and averaging over the statistical ensemble at thermodynamic equilibrium, they obtained the relation for the absorption coefficient:

$$k^c(\nu,T) = B(\Lambda'',\nu)R_c^2e^{-\frac{V_0(R_c)}{k_BT}}\left[\left(\frac{\mathbf{d}_1^2}{|\alpha_1|}+\frac{\mathbf{d}_2^2}{|\alpha_2|}\right)L^c_d(\Omega) + 2\frac{\mathbf{d}_1\mathbf{d}_2}{\sqrt{|\alpha_1\alpha_2|}}L^c_{\text{int}}(\Omega)\right]. \quad (33)$$

In O'Callaghan et al. [5], all calculations of spectral profiles $L^c_d(\Omega)$ and $L^c_{\text{int}}(\Omega)$ were made numerically, but in Devdariani and coworkers [2–4], the authors found analytical solutions based on the parabolic cylinder function $D_y(x)$.

In the case $\alpha_1\alpha_2 > 0$, both groups of authors obtained the same result for spectral profiles $L_d^c(\Omega) = 1$ and $L_{\text{int}}^c(\Omega) = 0$. As a consequence, the reduced absorption coefficient obtained using the semi-classical coupled channel approach SCCC is equal to that obtained using SCAA and SCDA, namely $k^c(\nu, T) = k^a(\nu, T) = k^d(\nu, T)$. This conclusion can be generalized to the spectrum in the neighborhood of the diabatic curves' crossing point R_c if this point is isolated from other crossing points and the condition $\frac{d}{dR}\Delta^d_{\Lambda'_1}(R)\frac{d}{dR}\Delta^d_{\Lambda'_2}(R)_{R=R_c} > 0$ is satisfied.

For $\alpha_1\alpha_2 < 0$, both groups of authors obtained a similar behavior of the profile functions $L_d^c(\Omega) = I_d(\Omega) + I_d(-\Omega) - P(\xi)$ and $L_{\text{int}}^c(\Omega) = I_{\text{int}}(\Omega) - I_{\text{int}}(-\Omega)$. The functions $L_d^c(\Omega)$ and $L_{\text{int}}^c(\Omega)$ have the same symmetry property concerning the sign of the frequency and the asymptotic behavior $L_d^c(\pm\infty) = 1$ and $L_{\text{int}}^c(\pm\infty) = L_{\text{int}}^c(0) = 0$, as well as the corresponding functions in the adiabatic representation. In Devdariani and coworkers [2–4], the functions $I_d(\Omega)$ and $I_{\text{int}}(\Omega)$ were calculated analytically as follows:

$$\begin{aligned} I_d(\Omega) &= \frac{1}{\pi^{1/2}}\int_0^\infty \frac{dx}{x^{1/2}} e^{x-\frac{3\pi}{2}\frac{\xi}{x^{1/2}}}\left|D_{-i\frac{\xi}{x^{1/2}}}\left(e^{i\frac{3\pi}{4}}\frac{\xi^{1/2}}{x^{1/4}}\Omega\right)\right|^2 \\ I_{\text{int}}(\Omega) &= \frac{2\xi^{1/2}}{\pi^{1/2}}\int_0^\infty \frac{dx}{x^{1/2}} e^{x-\frac{3\pi}{2}\frac{\xi}{x^{1/2}}}\,\text{Re}\left[e^{-i\frac{3\pi}{4}}D_{-i\frac{\xi}{x^{1/2}}}\left(e^{i\frac{3\pi}{4}}\frac{\xi^{1/2}}{x^{1/4}}\Omega\right)\overline{D}_{-i\frac{\xi}{x^{1/2}}-1}\left(e^{i\frac{3\pi}{4}}\frac{\xi^{1/2}}{x^{1/4}}\Omega\right)\right] \\ P(\xi) &= \frac{1}{\pi^{1/2}}\int_0^\infty \frac{dx}{x^{1/2}} e^{x-\frac{2\pi\xi}{x^{1/2}}} \end{aligned} \tag{34}$$

The function $P(\xi)$ refers to a temperature-averaged probability of a molecule moving in a potential of the initial diabatic electron state. Similarly, the probability of the molecule moving in the initial adiabatic state potential is $1 - P(\xi)$.

Figure 1a,c shows the spectral profiles $L_d(\xi, \Omega)$ and $L_{\text{int}}(\xi, \Omega)$, respectively, as functions of the frequency Ω and parameter ξ. Due to the symmetry properties, the spectral profiles are presented for positive frequencies Ω only. The maximum value of the profiles is near $\Omega = 2$, corresponding to the position of the minimum of the adiabatic state difference potential $\Delta^a_{\Lambda'1}$ (satellite rainbow). It can be seen that at low values of parameter ξ, both profiles tend toward the values of SCDA $L_d(\xi \to 0, \Omega) = 1$ and $L_{\text{int}}(\xi \to 0, \Omega) = 0$.

The differences of the spectral profiles in SCAA and SCCC $L_d^a(\xi, \Omega) - L_d(\xi, \Omega)$ and $L_{\text{int}}^a(\xi, \Omega) - L_{\text{int}}(\xi, \Omega)$ are shown in Figure 1b,d, respectively. It is seen that the differences between these two approaches are small or negligible for $\xi > 0.2$. The differences are slightly larger in the case of profiles $L_{\text{int}}(\xi, \Omega)$ but this is less important since it is very common that a scalar product $\mathbf{d}_1\mathbf{d}_2$ is small or equal to zero and the same holds for the second contribution in Equation (33). From Figure 1 it can be concluded that SCCC can be approximated for $\xi \ll 0.1$ using SCDA and for $\xi > 0.2$ using SCAA.

We can generalize the conclusion to any case of diabatic electronic states' potential crossing, as long as this crossing is isolated from other crossings and the condition $\frac{d}{dR}\Delta^d_{\Lambda'_1}(R)\frac{d}{dR}\Delta^d_{\Lambda'_2}(R)_{R=R_c} < 0$ is satisfied, and the Massey parameter is:

$$\xi = \frac{V(R_c)^2}{\hbar\left|\frac{d}{dR}\Delta_d(R)\right|_{R=R_c}}\sqrt{\frac{\mu}{2k_BT}}. \tag{35}$$

The criteria of applicability for SCAA and SCDA obtained in semi-classical theory can be applied to both quantum mechanical and semi-quantum approaches.

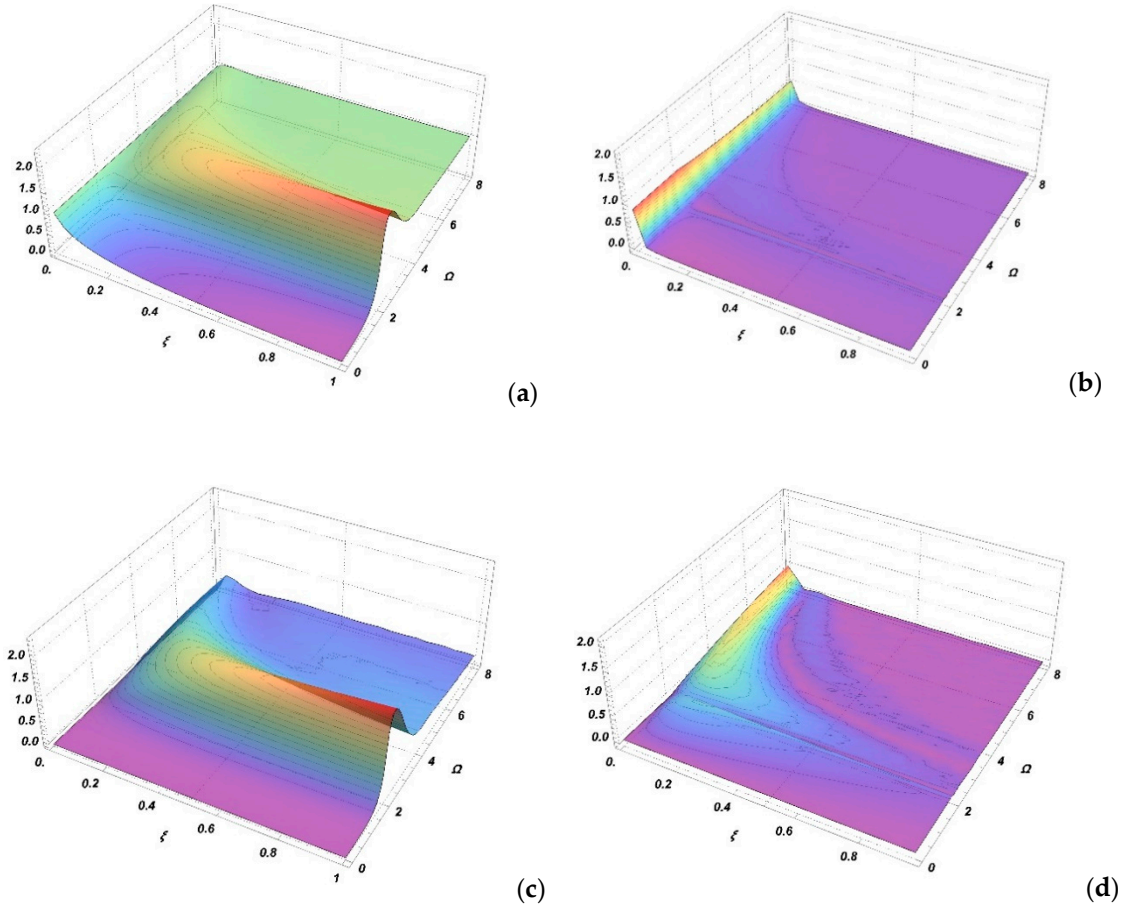

Figure 1. Absorption spectra contributions $L_d(\xi,\Omega)$ and $L_{\rm int}(\xi,\Omega)$ as a function of the Massey parameter ξ and reduced frequency Ω are shown in (**a**,**c**). The differences between these contributions and their adiabatic approximations $L_d^a(\xi,\Omega) - L_d(\xi,\Omega)$ and $L_{\rm int}^a(\xi,\Omega) - L_{\rm int}(\xi,\Omega)$ are shown in (**b**,**d**).

3. Results

3.1. Experiment

A T-type all-sapphire cell (ASC) of 4 cm in length and 1 cm in inner diameter was used for the transmission measurements in the K-Cs mixture vapor. The mixture in the sealed cell was 80% potassium and 20% cesium. The number density of atoms and molecules in the cell depends on the temperature at the tip of the side-arm finger (T_f) and the cell body (T_c). T_c was higher than T_f (at least 30 K) to prevent the condensation of the vapors on the inner side of the sapphire cell. The temperatures were controlled using two Chromel-Alumel Thermocouples.

In Figure 2a, we present the transmission intensities $I(\lambda,T)$ for several cells' T_c and finger T_f temperatures in the infrared spectral region between 900 nm and 1250 nm.

Assuming a low light intensity and a uniform medium inside the absorption cell of length L, using Beer-Lambert's Law $I(\lambda,T) = I_0(\lambda)e^{-L\cdot K(\lambda,T)}$, one can determine the linear absorption coefficient $K(\lambda,T) = \frac{1}{L}\ln\left(\frac{I_0(\lambda)}{I(\lambda,T)}\right)$, where $I_o(\lambda)$ is the intensity at the entrance of the cell. Following the measurements shown in Figure 2a, we approximated $I_o(\lambda) \approx I(\lambda, T_{c,f} = (542,533)K)$. The absorption coefficients for several temperatures are shown in Figure 2b.

Assuming the local thermodynamic equilibrium at an effective temperature T, the linear absorption coefficient of the mixture of potassium and cesium vapor for a low-pressure binary approximation was:

$$K(\lambda,T) = N_K(T)^2 k_{K_2}(\lambda,T) + N_{Cs}(T)^2 k_{Cs_2}(\lambda,T) + N_K(T)N_{Cs}(T)k_{KCs}(\lambda,T), \quad (36)$$

where $k_{K_2}(\lambda, T)$, $k_{Cs_2}(\lambda, T)$, and $k_{KCs}(\lambda, T)$ are the reduced absorption coefficients of K_2, Cs_2, and KCs molecules, respectively, and $N_K(T)$ and $N_{Cs}(T)$ are the number densities of K and Cs atoms, respectively. To analyze the spectra shown in Figure 2a,b, it was necessary to determine the reduced absorption coefficients of the K_2, Cs_2, and KCs molecules in the near-infrared part of the spectrum.

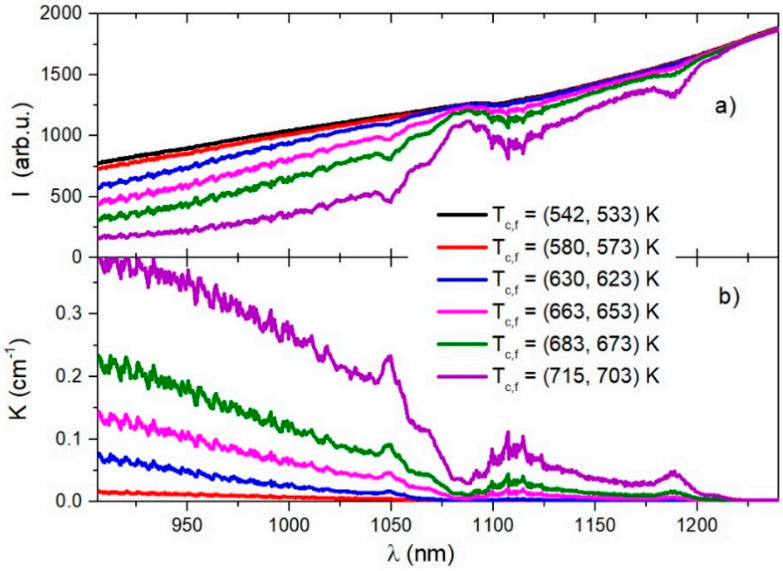

Figure 2. Relative intensity (in arbitrary units) of the light transmitted through a sapphire absorption cell at several temperatures $T_{c,f}$ is shown in (**a**). The alkali mixture absorption coefficients for the corresponding temperatures are shown in (**b**).

3.2. Near-Infrared Spectra of K_2, KCs, and Cs_2 Molecules

The dominant contribution to the near-infrared spectrum of alkali dimers is the $A - X$ band. This molecular band is the result of optical transitions between all rovibrational states of the excited $A^1\Sigma^+_{(u)}\left(0^+_{(u)}\right)$ (A state) and the ground $X^1\Sigma^+_{(g)}\left(0^+_{(g)}\right)$ electronic states (X state). The potential curve of the $A^1\Sigma^+_{(u)}\left(0^+_{(u)}\right)$ state crosses with the potential curve of the triplet electronic states $b^3\Pi_{(u)}\left(\Omega^{(+-)}_{(u)}\right)$. One component of the triplet state $b^3\Pi_{(u)}\left(0^+_{(u)}\right)$ (b state) is coupled with the A state via the matrix element of the SO interaction $\langle A|H_{SO}|b\rangle$. The electronic transition dipole moment for the $A - X$ transition is $\mathbf{d}(R) = \langle A|\hat{\mathbf{D}}(\mathbf{r}, R)|X\rangle$ and the $b - X$ transition is dipole-forbidden:$\langle b|\hat{\mathbf{D}}(\mathbf{r}, R)|X\rangle = 0$. The consequence of the $A - b$ coupling is the perturbation of the $A - X$ spectrum. In the case of heteronuclear KCs dimer, there is an allowed transition $b^3\Pi - a^3\Sigma^+$ but its contribution in the spectral region of interest is negligible and will not be analyzed in this study.

Most quantum-chemical ab-initio calculations are usually non-relativistic calculations in which the electronic Hamiltonian $\widetilde{H}_{el}(\mathbf{r}, R) = H_{el}(\mathbf{r}, R) - H_{SO}(\mathbf{r}, R)$ does not include SO interactions. As a result of these calculations, the electronic wavefunctions in Hund's case (a) are the representation and the corresponding electronic potentials, which are $V_X(R) = \left\langle X^1\Sigma^+_{(g)}\middle|\widetilde{H}_{el}\middle|X^1\Sigma^+_{(g)}\right\rangle$, and $V_A(R) = \left\langle A^1\Sigma^+_{(u)}\middle|\widetilde{H}_{el}\middle|A^1\Sigma^+_{(u)}\right\rangle$ and $\widetilde{V}_b(R) = \left\langle b^3\Pi_{(u)}\middle|\widetilde{H}_{el}\middle|b^3\Pi_{(u)}\right\rangle$, respectively. The SO interaction removes the triplet state $b^3\Pi_{(u)}\left(\Omega^{(+-)}_{(u)}\right)$ component's degeneration $\left\langle b^3\Pi_{(u)}\left(\Omega^{(+-)}_{(u)}\right)\middle|H_{el}\middle|b^3\Pi_{(u)}\left(\Omega^{(+-)}_{(u)}\right)\right\rangle = \widetilde{V}_b(R) + \frac{(\Omega-1)}{3}\delta_{3\Pi}(R)$ [42] such that the diabatic state b potential is $V_b(R) = \widetilde{V}_b(R) - \frac{1}{3}\delta_{3\Pi}(R)$. The $A - b$ coupling matrix element is $\langle A|H_{SO}|b\rangle = \frac{\sqrt{2}}{3}\delta_{fs}(R)$. Functions $\delta_{3\Pi}(R)$ and $\delta_{fs}(R)$ have the same asymptotic behavior, namely $\delta_{3\Pi}(\infty) = \delta_{fs}(\infty) = \delta$, where δ is the first doublet $P_{\frac{3}{2},\frac{1}{2}}$ fine structure splitting (potassium 57.7103 cm^{-1}, cesium 554.0388 cm^{-1}).

In References [20–33], the functions $\delta_{3\Pi}(R)$ and $\delta_{fs}(R)$ are fit to the Morse potential form and differ slightly at small interatomic distances. For the sake of simplicity, in this study, we used the approximation $\delta_{3\Pi}(R) = \delta_{fs}(R)$.

Using the diabatic states' wavefunctions and potentials, one can construct the corresponding adiabatic (α and β) state potentials and wavefunctions by diagonalizing matrix $\begin{pmatrix} V_A(R) & \frac{\sqrt{2}}{3}\delta_{fs}(R) \\ \frac{\sqrt{2}}{3}\delta_{fs}(R) & V_b(R) \end{pmatrix}$:

$$\begin{aligned} V_{\alpha,\beta}(R) &= \tfrac{1}{2}\left[V_A(R) + V_b(R) \pm \sqrt{\Delta_{Ab}(R)^2 + \tfrac{8}{9}\delta_{fs}(R)^2}\right] \\ \Phi_{\alpha,\beta}(r,R) &= \frac{1}{\sqrt{2}}\sqrt{1 \pm \frac{\Delta_{Ab}(R)}{\sqrt{\Delta_{Ab}(R)^2+\frac{8}{9}\delta_{fs}(R)^2}}}\Phi_A(r,R) \pm \frac{1}{\sqrt{2}}\sqrt{1 \mp \frac{\Delta_{Ab}(R)}{\sqrt{\Delta_{Ab}(R)^2+\frac{8}{9}\delta_{fs}(R)^2}}}\Phi_b(r,R) \end{aligned} \quad (37)$$

where $\Delta_{Ab}(R) = V_A(R) - V_b(R)$. Because the $b-X$ transition is dipole-forbidden, the adiabatic transition dipole moment $\alpha - X$ and $\beta - X$ transitions have the simple form:

$$\mathbf{d}_{\alpha,\beta}(R) = \frac{1}{\sqrt{2}}\sqrt{1 \pm \frac{\Delta_{Ab}(R)}{\sqrt{\Delta_{Ab}(R)^2 + \frac{8}{9}\delta_{fs}(R)^2}}}\mathbf{d}(R). \quad (38)$$

To obtain the electronic potential curves and transition dipole moments required in our calculations, we used existing theoretical and experimental data from the literature. In the case of the K_2 molecule, to construct potential curves, we combined ab-initio results [43], experimental data [19–21], and long-range region analytical results [44]. The spin–orbit function $\delta_{fs}(R)$ is taken from Manaa et al. [21] and the transition dipole moment was from Yan and Meyer [43]. For the KCs molecule, all data were taken from the Supplementary Materials of Borsalino et al. [33]. In the case of the Cs_2 molecule, for the diabatic state potentials, we used ab-initio results [45,46] (for states with 6S + 6P asymptote energies was shifted by +14 cm^{-1}) and experimental data [24,25]. In the long-range region, the potential curves were smoothly matched with analytical curves [44]. The function $\delta_{fs}(R)$ was taken from Bai et al. [25] and the transition dipole moment was from Allouche and Aubert-Frécon [47].

All relevant potential curves for K_2, KCs, and Cs_2 molecules are shown in Figure 3. It can be seen that the SO splitting function $\delta_{fs}(R)$ in the K_2 molecule was approximately ten times smaller than in the case of the KCs and Cs_2 molecules. The diabatic states' potential curves $V_A(R)$ and $V_b(R)$ had two well-separated crossing points for each molecule: K_2 (9.0 Bohr, 46.3 Bohr), KCs (9.6 Bohr, 20.9 Bohr), and Cs_2 (10.9 Bohr, 24.1 Bohr). In the same region, the potential curves of the adiabatic states avoided crossing.

At the long-range crossing point, $\frac{d}{dR}\Delta_A(R)\frac{d}{dR}\Delta_b(R)_{R=R_c} > 0$, where $\Delta_A(R) = V_A(R) - V_X(R)$ and $\Delta_b(R) = V_b(R) - V_X(R)$ are the difference potentials of the $A-X$ and $b-X$ transitions, respectively. According to the discussion in Section 2.3, in the neighborhood of the diabatic state potentials' crossing point, the adiabatic state difference potentials were monotonic functions and the absorption spectra could be found using a non-coherent adiabatic approximation.

Figure 4a–c shows the short-range region difference potentials of the $A-X$, $b-X$, $\alpha-X$, and $\beta-X$ transitions for the K_2, KCs, and Cs_2 molecules, respectively. At the short-range crossing point, $\frac{d}{dR}\Delta_A(R)\frac{d}{dR}\Delta_b(R)_{R=R_c} < 0$ and the difference potentials of the $\alpha-X$ and $\beta-X$ transitions had extrema in the neighborhood of the crossing point. As pointed out in Section 2.1 and Equation (16), the extremes of the difference potentials indicate the positions of the satellite rainbow in the spectrum. The difference potential of $\alpha-X$ had one minimum each at 985 nm, 1072 nm, and 1126 nm for the K_2, KCs, and Cs_2 molecules, respectively. The $\beta-X$ transition difference potential had maxima and minima at (996 nm, 1055 nm), (1107 nm, 1192 nm), and (1197 nm, 1205 nm) for K_2, KCs, and Cs_2, respectively. The minima of the $X-\beta$ transition difference potential approximately coincided with the minima of $A-X$ transition difference potential. Figure 4d–f shows the relevant transitions dipole moments. In the

neighborhood of the diabatic potentials' crossing point, the dipole moments of the $\alpha - X$ and $\beta - X$ transitions changed significantly with the interatomic distance, especially in the case of the K_2 dimer.

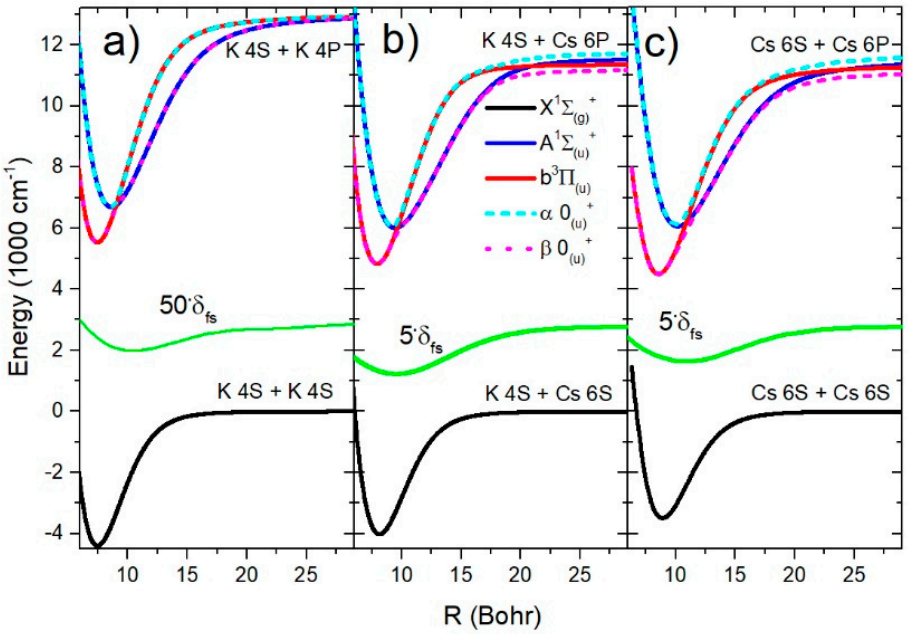

Figure 3. The electronic states' potentials curves relevant for the analysis of the infrared spectra of K_2, KCs, and Cs_2 molecules are shown in (**a**–**c**), respectively. The green curve shows the spin–orbit splitting function $\delta_{fs}(R)$ responsible for the coupling of the A and b states.

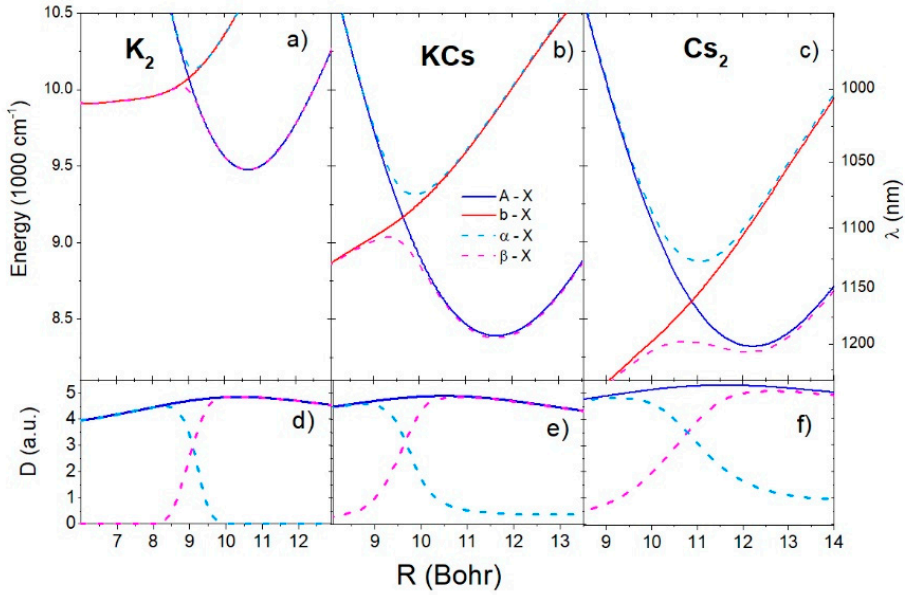

Figure 4. Difference potential curves of the A-X, b-X, α-X, and β-X transitions for K_2, KCs, and Cs_2 molecules are shown in (**a**–**c**), respectively. The corresponding transition dipole moments are shown in (**d**–**f**). The labels on the left side of the upper panel denote energy, and the right-side denotes the wavelength of the transition.

At the short-range crossing point R_c, the Massey parameter ξ at a typical experimental temperature 700 K is given in Table 1 for all dimers. The $A - b$ coupling for the K_2 dimer was much smaller than for Cs_2 even for the KCs dimer. In Table 1, the probability of atomic motion in diabatic potential $P(T)$ and the probability of atomic motion in adiabatic potential $1 - P(T)$ is given. It is evident that at the

temperature of 700 K, in the K_2 molecule, the atoms mainly moved in a diabatic potential, and for the KCs and especially Cs_2 molecules, movement was in an adiabatic potential.

Table 1. The first row gives the crossing points R_c of the potential curves of electronic states A and b for K_2, KCs, and Cs_2 molecules. In the second row, the Massey parameters at the crossing points for the temperature T = 700 K are given. In the third and fourth rows, the averaged probabilities P of atoms moving in diabatic potentials and the probabilities for atoms moving in adiabatic electronic potentials are given, respectively.

	K_2	KCs	Cs_2
R_c	9.0	9.57	10.87
ξ(700 K)	0.0051	0.21	0.75
P(700 K)	0.87	0.12	0.0056
1 − P(70 K)	0.13	0.88	0.9944

The behavior of the rotational B_ν constants also indicated the influence of the mixing of the two electronic states. The energy-dependent B_ν constants for A,b,α, and β, as well as the coupled A and b states for all dimers, are shown in Figure 5a–c. For the K_2 molecule, the coupled states B_ν constants were grouped around the diabatic states constants, but in the case of KCs and especially Cs_2 molecules, they were grouped around the adiabatic states B_ν constants. These facts are consistent with the Massey parameter shown in Table 1.

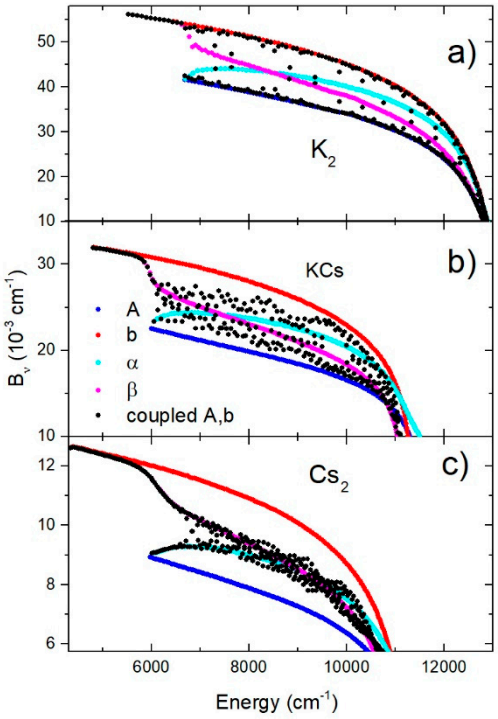

Figure 5. Constants of A, b, α, and β, as well as the coupled A and b electronic states, in the case of K_2, KCs, and Cs_2 molecules are shown in (**a**–**c**), respectively.

Using the full quantum (semi-quantum) approach, we calculated the reduced absorption coefficients for transitions between the X state and the coupled A and b states QCC (SQCC), non-coherent adiabatic approximation QAA (SQAA), and non-coherent diabatic approximation QDA (SQDA) of this transition. The rovibrational energies and radial wavefunctions were calculated using the FGH method via diagonalization of Hamiltonian matrices (Equations (10) and (22)). The number of grid points was N = 800 in the quantum mechanical calculation and N = 2000 in the semi-quantum calculation.

Using Equations (12) and (13), the rovibrational transition contributions were collected in bins of 0.4 nm and the spectra were smoothed using a Gaussian with a half-width of 0.9 nm for the quantum approach and 3.0 nm for the semi-quantum approach. Summation over the rotational quantum number J in the quantum approach was replaced by summation over the groups of n = 3 neighbor J values.

The numerical evaluation in this study was done using the Wolfram Mathematica 12.1 computing system. To calculate all the rovibrational contributions needed for the SQAA and SQDA spectra, 27 s of computer time was required, and for SQCC, 48 s was required. Using these data to calculate the absorption coefficient (Equation (13)) at a given temperature, 1 s of computer time was required for SQAA and SQCC, and 0.5 s was required for the SQDA spectra. For the full quantum mechanical approach, 340 s of computer time was required to calculate all the rovibrational contributions of the QAA and QDA spectra, and 830 s was required to calculate the QCC spectra. For the absorption coefficient evaluation at a given temperature, 70 s was required for the QCC and QAA spectra, and 38 s was required for the QDA spectra.

The reduced absorption coefficients at 700 K obtained using different approaches are shown in Figure 6. Each column in Figure 6 shows the different theoretical approaches for each of the dimers (K_2, KCs, Cs_2). The first row of Figure 6 shows the QCC and SQCC spectra, the second row shows the QAA and SQAA spectra, while the third row shows the QDA and SQDA spectra. It is noticeable that the non-coherent diabatic approximation (QDA, SQDA) gave an almost identical result as the coupled channel calculation (QCC, SQCC) in the case of K_2. In contrast, the non-coherent adiabatic approximation (QAA, SQAA) gave very similar results to the coupled channel calculation (QCC, SQCC) in the case of KCs and an almost identical result in the case of the Cs_2 molecule. Furthermore, excellent agreement of the semi quantum approximation (SQCC, SQAA, SQDA) with the full quantum calculation (QCC, QAA, QDA) was evident, especially in the case of the Cs_2 molecule.

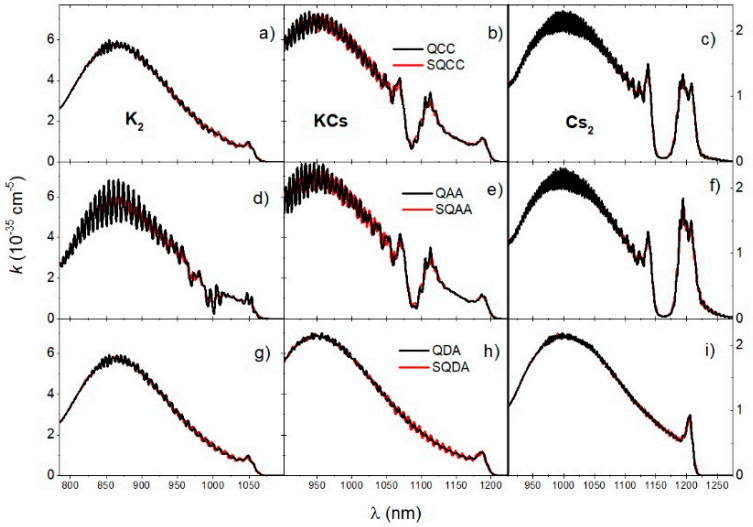

Figure 6. Reduced absorption coefficients of K_2, KCs, and Cs_2 molecules at temperature $T = 700K$ are shown in the first (**a**,**d**,**g**), second (**b**,**e**,**h**), and third columns (**c**,**f**,**i**), respectively. The first row (**a**–**c**) shows the QCC and SQCC spectra, the second row (**d**–**f**) shows the QAA and SQAA spectra, and the last row (**g**–**i**) shows the QDA and SQDA spectra.

3.3. The Comparison of the Experimental and Theoretical Absorption Coefficient

The absorption coefficient is temperature dependent, especially in the case of bound–bound transitions. Figure 7a–c shows the theoretical absorption coefficients of $A - X$ transition calculated using the QCC approach at several experimental temperatures for K_2, KCs, and Cs_2 molecules. Using Equation (36), we aimed to obtain the best fit of the experimental spectrum and theoretical simulation by iteratively changing the following parameters: temperature T, potassium atom number density N_K, and cesium atoms number density N_{Cs}. The iterative procedure started with the

experimental temperature but the best agreement was obtained at the end of the iteration with a temperature that was about 20 K higher than the initial one. Theoretical simulations were done for two temperatures, as shown in Figure 7d,e. The sapphire cell was filled with potassium and cesium in an approximate ratio of $N_K/N_{Cs} = 4.0$. Figure 7d,e show the results obtained for $N_K/N_{Cs} = 4.0$ and $N_K/N_{Cs} = 3.7$, respectively.

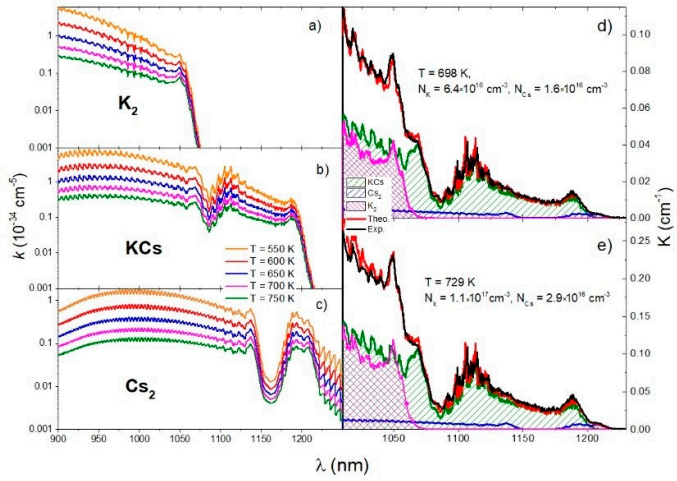

Figure 7. The first column shows the reduced absorption coefficients of K_2, KCs, and Cs_2 molecules (**a**–**c**, respectively) in the temperature range T = 550 K–750 K. The comparison of the experimental absorption coefficient (black curve) with the theoretical simulation (red curve) is in the second column (**d**,**e**). The theoretical simulations of the contributions of KCs, Cs_2, and K_2 molecules are shown in green, blue, and magenta, respectively.

In Figure 7d,e, the spectral contributions of K_2, KCs, and Cs_2 molecules calculated using the QCC approach are shown in magenta, green, and blue, respectively. By comparing the experimental and theoretical spectra, all important features in the experimental spectrum were identified. The peak at 1048.5 nm was related to the minimum of the K_2 $\alpha - X$ transition difference potential at 1055 nm. The shoulder at 1068 nm was related to the minimum of the KCs $\alpha - X$ transition difference potential at 1072 nm. The broad oscillating structure around 1106 nm was related to the maximum of the KCs $\beta - X$ transition difference potential at 1107 nm, and the peak at 1189 nm was related to the minimum at 1192 nm. The peak at 1208 nm was related to the minimum of the Cs_2 $\beta - X$ transition difference potential at 1205 nm.

4. Discussion and Conclusions

We studied the influence of the spin–orbit coupling of two excited diabatic electronic states of the same symmetry whose potential curves intersected on the high-temperature spectrum of the optical transition. In the neighborhood of the diabatic state potential curves' crossing point, the potential curves of the corresponding adiabatic states of the same symmetry avoided crossing and these states were mixed via the matrix element of radial non-adiabatic coupling. To obtain the correct spectrum of transitions from the isolated ground electronic state to the excited coupled diabatic or adiabatic states, the energies and wave functions of the excited states needed to be determined using a coupled channel calculus (QCC).

We distinguished two cases of the spectrum. In the neighborhood of an isolated diabatic state potential curves' crossing point, the transition difference potential curves of the excited adiabatic states were monotonic in the first case and had a minimum and a maximum in the second case. In the first case, based on the semi-classical analysis in Section 2.3, we concluded that a non-coherent adiabatic approach was a satisfactory approximation of the coupled channel calculation. Based on the discussion in Section 2.3, for the second case, we concluded that if the Massey parameter (Equation (35)) satisfied

$\xi << 0.1$, a non-coherent diabatic approach was a correct description of the spectrum, and if $\xi > 0.2$, a non-coherent adiabatic approach was justified. The potentials of the adiabatic electronic states are often available in the literature but there is no data on the corresponding diabatic state potentials and the spin–orbit mixing of these states. Assuming that the Landau–Zener approximation is valid in the neighborhood where the adiabatic state potentials avoided crossing, the Massey parameter can be written:

$$\xi = \frac{\Delta_a(R_c)^{3/2}}{4\hbar\left|\frac{d^2}{dR_2}\Delta_a(R)\right|^{1/2}_{R=R_c}}\sqrt{\frac{\mu}{2k_BT}} \tag{39}$$

where $\Delta_a(R)$ is the adiabatic state potentials difference, and the crossing point is defined via the condition $\frac{d}{dR}\Delta_a(R)_{R=R_c} = 0$. If only the adiabatic state potential curves are available, by using Equation (39), one can assess whether the non-coherent adiabatic approximation gives a satisfactory theoretical simulation of the spectrum.

The semi-quantum approach is extensively studied in References [1,15,18], and in this paper, we analyzed its applicability in coupled channel calculations. As discussed in References [1,15], the semi-quantum approximation describes the vibrational structure of the molecular band well but neglects the rotational structure. In the high-temperature, low-resolution spectra of molecules with a larger reduced mass, such as K_2, KCs, and Cs_2, the rotational structure was not resolved and the semi-quantum coupled channel approach had a very good agreement with the quantum coupled channel calculation.

Due to the low computer time consumption, a semi-quantum approach was found to be an appropriate tool for gas diagnostics. In our experimental study of a potassium and cesium vapor mixture absorption spectrum, we used the semi-quantum method to determine the atom's number density and temperature. The alkali mixture investigated in this article was suitable for analyzing the influence of the diabatic state SO coupling on the A–X transition spectrum. In the case of the K_2 molecule, due to the small SO interaction, the Massey parameter was small with $\xi = 0.0051$, and the non-coherent diabatic approximation described the spectrum well. In contrast, in the case of the Cs_2 molecule, the SO interaction and the Massey parameter were large with $\xi = 0.75$, and the spectrum could be calculated well using a non-coherent adiabatic approximation.

Low-resolution spectroscopy is applicable in the plasma diagnostics but can also be useful in the study of some fundamental phenomena and processes in the alkali gas. The experimental and theoretical methods presented here should also be applicable in the analysis of the SO interaction influence on the A-X transition spectra in the case of other heteronuclear alkali molecules, such as NaCs and RbCs.

Author Contributions: R.B. discussed the problem, analyzed the experiment, made the calculations, prepared the figures, and wrote the paper; G.P. made and analyzed the experiment, discussed the problem, and wrote the paper. All authors have read and agreed to the published version of the manuscript.

Funding: This research received no external funding.

Conflicts of Interest: The authors declare no conflict of interest.

References

1. Beuc, R.; Movre, M.; Pichler, G. High Temperature Optical Spectra of Diatomic Molecules at Local Thermodynamic Equilibrium. *Atoms* **2018**, *6*, 67. [CrossRef]
2. Девдариани, А.З.; Себякин Ю., Н. Температурная зависимость формы Ландау-Зинеровского сателита спектральной линии. *Опт.* иСпектр. **1976**, *48*, 1018–1021.
3. Девдариани, А.З.; Островский, В.Н.; Себякин, Ю.Н. Особенности в спектрах электронов и фотонов, сваязанныес взаимпдействием квазистационарных термов. ЖЕТϕ **1979**, *76*, 529–542.
4. Девдариани, А.З.; Себякин, Ю.Н. Оптическаяспектроскопия Ландау-Зинеровских переходов. ЖЕТϕ **1989**, *96*, 1997–2008.

5. O'Callaghan, M.J.; Gallagher, A.; Holstein, T. Absorption and emission of radiation in the region of an avoided level crossing. *Phys. Rev. A* **1985**, *32*, 2754–2768. [CrossRef] [PubMed]
6. Landau, L.D. On the theory of energy transmission in collisions I. *Phys. Z. Sowjet.* **1932**, *1*, 88.
7. Zener, C. Non-adiabatic crossing of energy levels. *Proc. R. Soc. Lond. A* **1932**, *137*, 696–702. [CrossRef]
8. Lam, L.K.; Gallagher, A.; Hessel, M.M. The intensity distribution in the Na_2 and Li_2 A–X bands. *J. Chem. Phys.* **1977**, *66*, 3550–3556. [CrossRef]
9. Chung, H.-K.; Kirby, K.; Babb, J.F. Theoretical study of the absorption spectra of the lithium dimer. *Phys. Rev. A* **1999**, *60*, 2002–2008. [CrossRef]
10. Erdman, P.S.; Larson, C.W.; Fajardo, M.; Sando, K.M.; Stwalley, W.C. Optical absorption of lithium metal vapor at high temperatures. *J. Quant. Spectrosc. Radiat. Transf.* **2004**, *88*, 447–481. [CrossRef]
11. Beuc, R.; Peach, G.; Movre, M.; Horvatić, B. Lithium, sodium and potassium resonance lines pressure broadened by helium atoms. *Astron. Astrophys. Trans.* **2018**, *30*, 315–322.
12. Chung, H.-K.; Kirby, K.; Babb, J.F. Theoretical study of the absorption spectra of the sodium dimer. *Phys. Rev. A* **2001**, *63*, 1–8. [CrossRef]
13. Vadla, C.; Beuc, R.; Horvatic, V.; Movre, M.; Quentmeier, A.; Niemax, K. Comparison of theoretical and experimental red and near infrared absorption spectra in overheated potassium vapor. *Eur. Phys. J. D* **2006**, *37*. [CrossRef]
14. Talbi, F.; Bouledroua, M.; Alioua, K. Theoretical determination of the potassium far-wing photoabsorption spectra. *Eur. Phys. J. D* **2008**, *50*, 141–151. [CrossRef]
15. Beuc, R.; Movre, M.; Horvatić, B. Time-efficient numerical simulation of diatomic molecular spectra. *Eur. Phys. J. D* **2014**, *68*. [CrossRef]
16. Beuc, R.; Movre, M.; Horvatic, V.; Vadla, C.; Dulieu, O.; Aymar, M. Absorption spectroscopy of the rubidium dimer in an overheated vapor: An accurate check of molecular structure and dynamics. *Phys. Rev. A* **2007**, *75*. [CrossRef]
17. Benedict, R.P.; Drummond, D.L.; Schlie, L.A. Fluorescence spectra and kinetics of Cs_2. *J. Chem. Phys.* **1979**, *70*, 3155. [CrossRef]
18. Horvatić, B.; Beuc, R.; Movre, M. Numerical simulation of dense cesium vapor emission and absorption spectra. *Eur. Phys. J. D* **2015**, *69*, 113. [CrossRef]
19. Ross, A.J.; Crozeti, P.; Effantint, C.; D'incani, J.; Barrow, R.F. Interactions between the $A^1\Sigma_u^+$ and $b^3\Pi_u$ states of K_2. *J. Phys. B* **1987**, *20*, 6225–6231. [CrossRef]
20. Lisdat, C.; Dulieu, O.; Knockel, H.; Tiemann, E. Inversion analysis of K_2 coupled electronic states with the Fourier grid method. *Eur. Phys. J. D* **2001**, *17*, 319–328. [CrossRef]
21. Manaa, M.R.; Ross, A.J.; Martin, F.; Crozet, P.; Lyyra, A.M.; Li, L.; Amiot, C.; Bergeman, T. Spin–orbit interactions, new spectral data, and deperturbation of the coupled $b^3\Pi_u$ and $A^1\Sigma_u^+$ states of K_2. *J. Chem. Phys.* **2002**, *117*, 11208. [CrossRef]
22. Salami, H.; Bergeman, T.; Beser, B.; Bai, J.; Ahmed, E.H.; Kotochigova, S.A.; Lyyra, M.; Huennekens, J.; Lisdat, C.; Stolyarov, A.V.; et al. Spectroscopic observations, spin-orbit functions, and coupled-channel deperturbation analysis of data on the $A^1\Sigma_u^+$ and $b^3\Pi_u$ of Rb_2. *Phys. Rev. A* **2009**, *80*, 022515. [CrossRef]
23. Drozdova, A.N.; Stolyarov, A.V.; Tamanis, M.; Ferber, R.; Crozet, P.; Ross, A.J. Fourier transform spectroscopy and extended deperturbation treatment of the spin-orbit-coupled co $A^1\Sigma_u^+$ and $b^3\Pi_u$ states of the Rb_2 molecule. *Phys. Rev. A* **2013**, *88*, 022504. [CrossRef]
24. Verges, J.; Amiot, C. The Cs_2 $A^1\Sigma_u^+ \rightarrow X^1\Sigma_g^+$ fluorescence excited by the Ar^+ 1.09-μm laser line. *J. Mol. Spectrosc.* **1987**, *126*, 393–404. [CrossRef]
25. Bai, J.; Ahmed, E.H.; Beser, B.; Guan, Y.; Kotochigova, S.; Lyyra, A.M.; Ashman, S.; Wolfe, C.M.; Huennekens, J.; Xie, F.; et al. Global analysis of data on the spin-orbit-coupled $A^1\Sigma_u^+$ and $b^3\Pi_u$ states of Cs_2. *Phys. Rev. A* **2011**, *83*, 032514. [CrossRef]
26. Kowalczyk, P.; Jastrzebski, W.; Szczepkowski, J.; Pazyuk, E.A.; Stolyarov, A.V. Direct coupled-channels deperturbation analysis of the $A^1\Sigma^+ \sim b^3\Pi$ complex in LiCs with experimental accuracy. *J. Chem. Phys.* **2015**, *142*, 234308. [CrossRef] [PubMed]
27. Grochola, A.; Szczepkowski, J.; Jastrzebski, W.; Kowalczyk, P. Study of the $A^1\Sigma^+$ and $b^3\Pi(0)$ states in LiCs by a polarization labelling spectroscopy technique. *J. Quant. Spectrosc. Radiat. Transf.* **2014**, *145*, 147–152. [CrossRef]

28. Zaharova, J.; Tamanis, M.; Ferber, R.; Drozdova, A.N.; Pazyuk, E.A.; Stolyarov, A.V. Solution of the fully-mixed-state problem: Direct deperturbation analysis of the $A^1\Sigma^+$–$b^3\Pi$ complex in a NaCs dimer. *Phys. Rev. A* **2009**, *79*, 012508. [CrossRef]
29. Bergeman, T.; Fellows, C.E.; Gutterres, R.F.; Amiot, C. Analysis of strongly coupled electronic states in diatomic molecules: Low-lying excited states of RbCs. *Phys. Rev. A* **2003**, *67*, 050501(R). [CrossRef]
30. Docenko, O.; Tamanis, M.; Ferber, R.; Bergeman, T.; Kotochigova, S.; Stolyarov, A.V.; Nogueira, A.; Fellows, C.E. Spectroscopic data, spin-orbit functions, and revised analysis of strong perturbative interactions for the $A^1\Sigma^+$ and $b^3\Pi$ states of RbCs. *Phys. Rev. A* **2010**, *81*, 042511. [CrossRef]
31. Kruzins, A.; Klincare, I.; Nikolayeva, O.; Tamanis, M.; Ferber, R.; Pazyuk, E.A.; Stolyarov, A.V. Fourier-transform spectroscopy of (4) $^1\Sigma^+ \rightarrow A^1\Sigma^+ \rightarrow b^3\Pi, A^1\Sigma^+ \rightarrow b^3\Pi \rightarrow {}^1\Sigma^+$, $(1)^3\Delta_1 \rightarrow b^3\Pi_{0\pm}$ transitions in KCs and deperturbation treatment of $A^1\Sigma^+$ and $b^3\Pi$. *J. Chem. Phys.* **2013**, *139*, 244301. [CrossRef] [PubMed]
32. Tamanis, M.; Klincare, I.; Kruzins, A.Ž.; Nikolayeva, O.; Ferber, R.; Pazyuk, E.A.; Stolyarov, A.V. Direct excitation of the "dark" $b^3\Pi$ state predicted by deperturbation analysis of the $A^1\Sigma^+$–$b^3\Pi$ complex in KCs. *Phys. Rev. A* **2010**, *82*, 032506. [CrossRef]
33. Borsalino, D.; Vexiau, R.; Aymar, M.; Luc-Koenig, E.; Dulieu, O.; Bouloufa-Maafa, N. Prospects for the formation of ultracold polar ground state KCs molecules via an optical process. *J. Phys. B* **2016**, *49*, 055301. [CrossRef]
34. Janev, R.K. Nonadiabatic Transitions between Ionic and Covalent States. *Adv. At. Mol. Phys.* **1976**. [CrossRef]
35. Lichten, W. Resonant Charge Exchange in Atomic Collisions. *Phys. Rev.* **1963**, *131*, 229. [CrossRef]
36. Smith, F.T. Diabatic and Adiabatic Representations for Atomic Collision Problems. *Phys. Rev.* **1969**, *179*, 111. [CrossRef]
37. Colbert, D.T.; Miller, W.H. A novel discrete variable representation for quantum mechanical reactive scattering via the S -matrix Kohn method. *J. Chem. Phys.* **1992**, *96*, 1982–1991. [CrossRef]
38. Lam, K.; George, T.F. Semiclassical approach to spontaneous emission of molecular collision systems: A dynamical theory of fluorescence line shapes. *J. Chem. Phys.* **1982**, *76*, 3396. [CrossRef]
39. Beuc, R.; Horvatic, V. The investigation of the satellite rainbow in the spectra of diatomic molecules. *J. Phys. B* **1992**, *25*, 1497–1510. [CrossRef]
40. Kokoouline, V.; Dulieu, O.; Kosloff, R.; Masnou-Seeuws, F. Theoretical treatment of channel mixing in excitedRb_2 and Cs_2 ultracold molecules: Determination of predissociation lifetimes with coordinate mapping. *Phys. Rev. A* **2000**, *62*. [CrossRef]
41. Beuc, R.; Movre, M.; Mihajlov, A.A. Nonadiabatic affects in absorption line shape. In Proceedings of the 9th International Conference on Spectral Line Shapes, Torun, Poland, 25–29 July 1988; p. D11.
42. Ovchinnikova, M.Y. Transitions between fine-structure components in resonance interactions for alkali metals. *Theor. Exp. Chem.* **1965**, *1*, 12–16. [CrossRef]
43. Yan, L.; Meyer, W. Electronic state potential curves and electronic transition dipole moments of K_2 molecules. Unpublished Results.
44. Marinescu, M.; Dalgarno, A. Dispersion forces and long-range electronic transition dipole moments of alkali-metal dimer excited states. *Phys. Rev. A* **1995**, *52*, 311. [CrossRef] [PubMed]
45. Spies, N. Theoretische Untersuchung von Elektronisch Angeregten Zuständen der Moleküle Li_2 und Cs_2. Ph.D. Thesis, Fachbereich Chemie, Kaiserslautern University, Kaiserslautern, Germany, 1990.
46. Meyer, W.; Spies, N. Electronic State Potential Curves of Cs_2 Molecules. Unpublished Results.
47. Allouche, A.R.; Aubert-Frécon, M. Transition dipole moments between the low-lying $\Omega_{g,u}^{+/-}$ states of the Rb_2 and Cs_2 molecules. *J. Chem. Phys.* **2012**, *136*, 114302. [CrossRef] [PubMed]